Prepared for submission to JHEP

$B_s \to \mu^+\mu^-$ in a Two-Higgs-Doublet Model with flavour-changing up-type Yukawa couplings

Martin S. Lang, Ulrich Nierste

Institute for Theoretical Particle Physics, Karlsruhe Institute of Technology (KIT), Wolfgang-Gaede-Str. 1, D-76131 Karlsruhe, Germany

E-mail: m.lang@kit.edu, ulrich.nierste@kit.edu

Abstract: We present a Two-Higgs-Doublet Model in which the structure of the quark Yukawa sector is governed by three spurions breaking the flavour symmetries. The model naturally suppresses FCNC amplitudes in the down-type sector, but permits sizable FCNC couplings in the up sector. We calculate the branching ratio of $B_s \to \mu^+\mu^-$ to leading and next-to-leading order of QCD for the case with FCNC couplings of the heavy neutral Higgs bosons to top and charm quarks and verify that all counterterms follow the pattern dictated by the spurion expansion of the Yukawa matrices. We find correlations between $B_s \to \mu^+\mu^-$, $b \to s\gamma$, and the Higgs masses. The $B_s - \bar{B}_s$ mixing amplitude is naturally suppressed in the model but can probe a portion of the parameter space with very heavy Higgs bosons.

Contents

1 Introduction

Two-Higgs-Doublet models (2HDMs) [1, 2] are a popular extension of the Standard Model (SM) due to their relative simplicity, involving no additional particles apart from a second Higgs doublet. Moreover, a strong motivation to study 2HDMs also comes from theories in which a second Higgs doublet is required due to symmetry arguments, e.g. axion models in the context of the strong CP puzzle [3–5] or minimal supersymmetry [6]. 2HDMs differ in the structure of Higgs-fermion Yukawa couplings. The historically most favoured variant is the so-called type-II 2HDM in which up- and down-type quarks couple to separate Higgs doublets exclusively. In most of the 2HDMs, flavour-changing neutral current processes such as the decay $B_s \to \mu^+\mu^-$ are loop-suppressed and therefore small masses of the additional Higgs bosons are in principle possible, an appealing feature during the early LHC searches. A general 2HDM exhibits, however, a much richer Yukawa structure [7, 8], in which flavour-changing neutral Higgs-boson couplings are possible, in case quarks couple to multiple Higgs doublets at the same time.

In this paper, we will consider the rare decay $B_s \to \mu^+\mu^-$ in the context of a 2HDM with more general Yukawa couplings. The model under consideration will feature flavour-changing up-type Yukawa couplings of the additional neutral Higgs bosons, most notably a charm-top transition which may eliminate the Cabibbo-Kobayashi-Maskawa (CKM) suppression that is present in both the SM and the 2HDM type-II models. We put special emphasis on the leading corrections for large values of $\tan\beta$.

The outline of the paper is as follows: In section 2, we will introduce the effective operators contributing to the low-energy weak $B_s \to \mu^+\mu^-$ decay. The Yukawa and Higgs sectors of the 2HDM are presented in section 3, while section 4 is dedicated to a short description of the computational setup used for the evaluation Feynman diagrams. The limiting case of the type-II 2HDM is introduced in section 5, with the additional contributions from flavour-changing neutral-Higgs Yukawa couplings being presented in section 6. Finally, we will discuss the phenomenology of such models in section 7, before summarizing in section 8.

2 The decay $\mathbf{B_s} \to \mu^+\mu^-$

The typical momentum scale for B_s decays is of order M_{B_s} or smaller, so that weak B_s decays can be described by an effective theory in which the heavy W, Z bosons, the top quark, and the Higgs bosons of the 2HDM are integrated out. The resulting $|\Delta B| = 1$ Hamiltonian H_{eff} describes the interactions mediated by these heavy particles in terms of dimension-6 operators changing the beauty quantum number B by one unit. The piece of H_{eff} relevant for $B_s \to \mu^+\mu^-$ reads

$$H_{\text{eff}} = N \sum_{i=A,S,P} \left(C_i Q_i + C_i' Q_i'\right) . \tag{2.1}$$

The operators in Eq. (2.1) are

$$\begin{aligned}
Q_A &= \left(\bar{b}\gamma_\mu P_L s\right)\left(\bar{\mu}\gamma^\mu\gamma_5\mu\right) , & Q_A' &= \left(\bar{b}\gamma_\mu P_R s\right)\left(\bar{\mu}\gamma^\mu\gamma_5\mu\right) , \\
Q_S &= \left(\bar{b}P_L s\right)\left(\bar{\mu}\mu\right) , & Q_S' &= \left(\bar{b}P_R s\right)\left(\bar{\mu}\mu\right) , \\
Q_P &= \left(\bar{b}P_L s\right)\left(\bar{\mu}\gamma_5\mu\right) , & Q_P' &= \left(\bar{b}P_R s\right)\left(\bar{\mu}\gamma_5\mu\right) ,
\end{aligned} \tag{2.2}$$

and are multiplied with their respective *Wilson coefficients* $C_A, \dots, C_P'$ which contain the dependence on the heavy masses. The normalisation factor in Eq. (2.1) is

$$N = \frac{G_F^2 M_W^2}{\pi^2} V_{ts} V_{tb}^* = \frac{G_F \alpha_{\text{em}}(\mu)}{\sqrt{2}\pi \sin^2\theta_w} V_{ts} V_{tb}^*, \tag{2.3}$$

which complies with the conventions of Ref. [9]. The second "=" sign only holds to lowest order in the electroweak interaction, while in higher orders the relation between the Fermi constant G_F and the electromagnetic coupling $\alpha_{\text{em}} = e^2/(4\pi)$, the weak mixing angle θ_w and the W mass M_W is modified. Electroweak corrections have been calculated in Ref. [10] and e.g. remove the ambiguities related to the choice of the renormalisation scheme for these parameters; in the second version for N in Eq. (2.3) this issue also includes the choice of the scale in the running $\alpha_{\rm em}$. We choose the first definition $N \propto G_F^2$ in this paper, for which the electroweak corrections to the SM contribution to C_A are as small as -2.4% [10].

We introduce the perturbative expansion of the C_i as

$$C_i = C_i^{(0)} + \left(\frac{\alpha_s}{4\pi}\right) C_i^{(1)} + \dots\,, \tag{2.4}$$

where $C_i^{(0)}$ denotes the leading order (LO), arising in the SM from one-loop electroweak diagrams. $C_i^{(1)}$ comprises the next-to-leading order (NLO) QCD corrections. In the SM only C_A is relevant, C'_A is suppressed w.r.t. C_A by the ratio $m_b m_s/M_W^2$ involving strange and bottom masses $m_{\{s,b\}}$ and $C^{(\prime)}_{S,P}$ receive additional suppression factors of $M_{B_s}^2/M_W^2$. The leading contributions $C_i^{(1)}$ arise from one-loop electroweak diagrams at order G_F^2 in the SM, hence the branching ratio is rather small.

The average time-integrated branching ratio is given by [11, 12]

$$\overline{\mathcal{B}}\left(B_s \to \mu^+\mu^-\right) = |N|^2 \frac{M_{B_s}^3 f_{B_s}^2}{8\pi\Gamma_H^s}\beta\left[\left|r\left(C_A - C'_A\right) - u\left(C_P - C'_P\right)\right|^2 F_P + \left|u\beta\left(C_S - C'_S\right)\right|^2 F_S\right]\,, \tag{2.5}$$

with dimensionless quantities

$$r = \frac{2m_\mu}{M_{B_s}}\,, \qquad \beta = \sqrt{1-r^2}\,, \qquad u = \frac{M_{B_s}}{m_b + m_s}\,. \tag{2.6}$$

Here, Γ_H^s (Γ_L^s) denotes the decay width of the heavier (lighter) B_s mass eigenstate, and the factors F_P and F_S account for the mixing of the B_s-$\bar{B}_s$ system, given by

$$\begin{aligned} F_P =& 1 - \frac{\Gamma_L^s - \Gamma_H^s}{\Gamma_L^s}\sin^2\left[\arg\left(r\left(C'_A - C_A\right) - u\left(C'_P - C_P\right)\right)\right]\,, \\ F_S =& 1 - \frac{\Gamma_L^s - \Gamma_H^s}{\Gamma_L^s}\cos^2\left[\arg\left(C'_S - C_S\right)\right] \end{aligned} \tag{2.7}$$

in the absence of significant CP-violating New Physics contributions to the $B_s - \bar{B}_s$ mixing amplitude. In writing Eq. (2.5), we have used the pseudoscalar decay constant f_{B_s} to rewrite the operator matrix elements as

$$\begin{aligned} \langle 0|\bar{b}\gamma_\mu\gamma_5 s|B_s(p)\rangle =& \, \mathrm{i}p_\mu f_{B_s}\,, \\ \langle 0|\bar{b}\gamma_5 s|B_s(p)\rangle =& -\mathrm{i}f_{B_s}\frac{M_{B_s}^2}{m_b + m_s}\,, \end{aligned} \tag{2.8}$$

where the second equation follows from the first one by use of the Dirac equation.

3 2HDM with suppressed down-type FCNC couplings

3.1 General Yukawa sector

The Yukawa Lagrangian of the general ("type III") 2HDM reads

$$\begin{aligned} L_Y =& -\overline{Q}'_f\left[\overline{Y}^d_{fi}H_d + \overline{\epsilon}^d_{fi}H_u\right]d'_{iR} - \overline{Q}'_f\left[\overline{Y}^u_{fi}\epsilon H_u^* + \overline{\epsilon}^u_{fi}\epsilon H_d^*\right]u'_{iR} + h.c. \\ \equiv& -\overline{Q}'\left[\overline{Y}^d H_d + \overline{\epsilon}^d H_u\right]d'_R - \overline{Q}'\left[\overline{Y}^u\epsilon H_u^* + \overline{\epsilon}^u\epsilon H_d^*\right]u'_R + h.c. \end{aligned} \tag{3.1}$$

with

$$H_{u,d} = \begin{pmatrix} H^+_{u,d} \\ H^0_{u,d} \end{pmatrix} \qquad \epsilon H^*_{u,d} = \begin{pmatrix} H^{0*}_{u,d} \\ -H^-_{u,d} \end{pmatrix} \tag{3.2}$$

$$\text{and} \quad Q'_f = \begin{pmatrix} u'_{fL} \\ d'_{fL} \end{pmatrix}. \tag{3.3}$$

The subscripts $f, i = 1, 2, 3$ label the generations, e.g. $u'_{3L} = t'_L$. The notation in Eq. (3.1) follows Ref. [8], except that our H_d corresponds to $-\epsilon H^*_d$ of that paper.

The vacuum expectation values (vevs) and related quantities are

$$\langle H^0_u \rangle = v_u = v \sin\beta, \qquad \langle H^0_d \rangle = v_d = v \cos\beta,$$

$$\tan\beta := \frac{v_u}{v_d}, \qquad v := \sqrt{v_u^2 + v_d^2} = 174\,\text{GeV}. \tag{3.4}$$

The quark mass matrices are

$$M^d = \overline{Y}^d v \cos\beta + \overline{\epsilon}^d v \sin\beta, \qquad M^u = \overline{Y}^u v \sin\beta + \overline{\epsilon}^u v \cos\beta, \tag{3.5}$$

which we diagonalise in the usual way:

$$u'_{L,R} = S^u_{L,R} u_{L,R}, \qquad d'_{L,R} = S^d_{L,R} d_{L,R}, \tag{3.6}$$

$$S^{d\dagger}_L M^d S^d_R = \hat{M}^d = \begin{pmatrix} m_d & 0 & 0 \\ 0 & m_s & 0 \\ 0 & 0 & m_b \end{pmatrix}, \qquad S^{u\dagger}_L M^u S^u_R = \hat{M}^u = \begin{pmatrix} m_u & 0 & 0 \\ 0 & m_c & 0 \\ 0 & 0 & m_t \end{pmatrix}, \tag{3.7}$$

with the unprimed fields corresponding to quark mass eigenstates. The gauge sector of the 2HDM is invariant under independent unitary rotations of the fields Q', d'_R, and u'_R in flavour space. We use Eq. (3.6) and choose

$$Q' \equiv S^d_L Q \tag{3.8}$$

and find L_Y in the so-called *down basis*:

$$L_Y \equiv -\overline{Q}\left[Y^d H_d + \epsilon^d H_u\right] d_R \; - \; \overline{Q}\left[Y^u \epsilon H^*_u + \epsilon^u \epsilon H^*_d\right] u_R + h.c. \tag{3.9}$$

with the appropriately transformed Yukawa matrices

$$Y^{u,d} = S^{d\dagger}_L \overline{Y}^{u,d} S^{u,d}_R, \qquad \epsilon^{u,d} = S^{d\dagger}_L \overline{\epsilon}^{u,d} S^{u,d}_R \tag{3.10}$$

and the CKM matrix

$$V = S^{u\dagger}_L S^d_L. \tag{3.11}$$

The Yukawa Lagrangian L_Y in Eq. (3.9) is manifestly SU(2) invariant, with the SU(2) doublet

$$Q = S^{d\dagger}_L Q' = \begin{pmatrix} V^\dagger u_L \\ d_L \end{pmatrix}.$$

Eq. (3.9) is our starting point; the Yukawa matrices are related to the diagonal mass matrices as

$$\frac{\hat{M}_d}{v} = Y^d \cos\beta + \epsilon^d \sin\beta, \qquad \frac{\hat{M}_u}{v} = V\left(Y^u \sin\beta + \epsilon^u \cos\beta\right). \tag{3.12}$$

Non-vanishing off-diagonal entries of $Y^{d,u}$, $\epsilon^{d,u}$ give rise to FCNC couplings of the neutral components of the Higgs doublets.

In a general 2HDM the quantity $\tan\beta$ has no physical meaning: One can arbitrarily rotate $\left(H_u, H_d\right)$ in Eq. (3.1) leading to a Lagrangian of the same form (yet with different Yukawa matrices) and the rotation angle will add to β. The situation is different in variants of the 2HDM in which H^u and H^d are distinguished by quantum numbers which forbid such rotations of $\left(H_u, H_d\right)$. Prominent examples are the 2HDM of type I and II, in which two out of the four Yukawa matrices in Eqs. (3.1) and (3.9) are absent. The type-I model corresponds to $\epsilon^d = Y^u = 0$. The type-II model is instead found for $\epsilon^d = \epsilon^u = 0$.

The doublets $\phi_{\rm SM}$, $\phi_{\rm new}$ of the *Higgs basis* [13–15] are defined by a rotation of the two doublets H_u and H_d by the angle β such that $\phi_{\rm new}$ has no vev:

$$\begin{pmatrix} \phi_{\rm new} \\ \phi_{\rm SM} \end{pmatrix} = \begin{pmatrix} \cos\beta & -\sin\beta \\ \sin\beta & \cos\beta \end{pmatrix} \begin{pmatrix} H_u \\ H_d \end{pmatrix} \tag{3.13}$$

One has

$$\phi_{\rm SM} = \begin{pmatrix} G^+ \\ v + \dfrac{\phi^0 + iG^0}{\sqrt{2}} \end{pmatrix}, \qquad \phi_{\rm new} = \begin{pmatrix} H^+ \\ \dfrac{\phi^{0\prime} + iA^0}{\sqrt{2}} \end{pmatrix}. \tag{3.14}$$

Next we use Eq. (3.13) to express L_Y in terms of $\phi_{\rm SM}$ and $\phi_{\rm new}$:

$$\begin{aligned} L_Y = \; & \overline{Q}\Big[-Y^d\cos\beta - \epsilon^d \sin\beta\Big]\phi_{\rm SM} d_R \quad + \overline{Q}\Big[Y^d \sin\beta - \epsilon^d\cos\beta\Big]\phi_{\rm new} d_R \\ & + \overline{Q}V^\dagger\Big[-Y^u \sin\beta - \epsilon^u\cos\beta\Big]\epsilon\phi^*_{\rm SM} u_R + \overline{Q}V^\dagger\Big[-Y^u\cos\beta + \epsilon^u\sin\beta\Big]\epsilon\phi^*_{\rm new} u_R + h.c. \end{aligned} \tag{3.15}$$

By using Eq. (3.5) to eliminate Y^u and Y^d one can write the couplings to physical charged and neutral Higgs bosons in Eq. (3.15) as

$$\begin{aligned} \mathcal{L}_Y^{\rm phys} = & -\bar{u}_L\left[\frac{\hat{M}^u}{v}\cot\beta + g^u\right]u_R\frac{\phi^{0\prime} - {\rm i}A^0}{\sqrt{2}} + \bar{d}_L\left[\frac{\hat{M}^d}{v}\tan\beta + g^d\right]d_R\frac{\phi^{0\prime} + {\rm i}A^0}{\sqrt{2}} \\ & + \bar{u}_L V\left[\frac{\hat{M}^d}{v}\tan\beta + g^d\right]d_R H^+ + \bar{d}_L V^\dagger\left[\frac{\hat{M}^u}{v}\cot\beta + g^u\right]u_R H^- \\ & - \bar{d}_L\frac{\hat{M}^d}{v}d_R\left(v + \frac{\phi^0}{\sqrt{2}}\right) - \bar{u}_L\frac{\hat{M}^u}{v}u_R\left(v + \frac{\phi^0}{\sqrt{2}}\right) + h.c. \end{aligned} \tag{3.16}$$

with the matrices [8]

$$g^d = -\epsilon^d \sin\beta\left(\tan\beta + \cot\beta\right), \qquad g^u = -\epsilon^u\cos\beta\left(\tan\beta + \cot\beta\right). \tag{3.17}$$

The non-diagonal matrices g^d and g^u characterise the deviations from the popular type-II 2HDM (for which $g^d = g^u = 0$) and can induce flavour-changing couplings of neutral Higgs bosons. Note that the type-I model is also included in the formalism and recovered by using Eq. (3.5) with $Y^u = 0$ in the expression for g^d. For our loop calculation and the phenomenological analysis it is advantageous to work with $g^{d,u}$ rather than $\epsilon^{d,u}$, especially for the definition of the renormalisation prescriptions. We write $g^d_{ij} = g_{d_i d_j}$, where d_i is the i-th down-type quark flavor, $i = 1, 2, 3$, and similarly for g^u.

We are interested in 2HDM scenarios in which current and forthcoming measurements by LHCb and CMS can find deviations in $B(B_s \to \mu^+\mu^-)$ from the SM prediction. This consideration guides us to lepton Yukawa couplings of the type-II form,

$$\mathcal{L}_Y^l = +\bar{l}_L \left[\frac{\hat{M}^l}{v} \tan\beta\right] l_R \frac{\phi^{0\prime} + \mathrm{i}A^0}{\sqrt{2}} + \bar{\nu}_L \left[\frac{\hat{M}^l}{v} \tan\beta\right] l_R H^+ + h.c. \tag{3.18}$$

and large values of $\tan\beta$ to enhance the muon Yukawa coupling $Y_\mu = m_\mu/v \tan\beta$ over its SM value. $\hat{M}^l$ in Eq. (3.18) denotes the diagonal mass matrix of the charged leptons.

We restrict ourselves to the CP-conserving Higgs potential, in which diagrams involving A^0 contribute to the Wilson coefficient C_P, while diagrams with the CP-even neutral Higgs states contribute to C_S. The two Higgs bosons ϕ^0 and $\phi^{0\prime}$ are in general not mass eigenstates. The latter are given by

$$\begin{pmatrix} h^0 \\ H^0 \\ A^0 \end{pmatrix} = \begin{pmatrix} \sin(\beta-\alpha) & \cos(\beta-\alpha) & 0 \\ \cos(\beta-\alpha) & -\sin(\beta-\alpha) & 0 \\ 0 & 0 & 1 \end{pmatrix} \begin{pmatrix} \phi^0 \\ \phi^{0\prime} \\ A^0 \end{pmatrix}. \tag{3.19}$$

The angle α is an a priori arbitrary parameter of the theory that serves to diagonalise the mass matrix of neutral Higgs bosons.

3.2 Spurion expansion

The 2HDM of type I and II (and their variants with modified lepton couplings) invoke (softly broken) $\mathbb{Z}_2$ symmetries to forbid FCNC couplings of the neutral Higgs bosons. This was motivated by the wish to find non-standard Higgs bosons at modern colliders, because for generic values of the Yukawa matrices in Eq. (3.9) constraints from FCNC processes like meson-antimeson mixing push these masses to values outside the reach of of LEP, Tevatron, and LHC. With the absence of discoveries of non-standard Higgs bosons this line of arguments loses its appeal and the consideration of more general Yukawa sectors is in order.

The type-II model is the most studied variant of the 2HDM for two reasons: Firstly, it constitutes the tree-level Higgs sector of the Minimal Supersymmetric Standard Model (MSSM), in which the holomorphy of the superpotential enforces $\epsilon^{u,d} = 0$. Secondly, the type-II model is phenomenologically especially interesting, because in this model FCNC processes are sensitive to loop effects of the charged Higgs boson. A prominent example of the latter feature is the branching ratio $\mathcal{B}(B \to s\gamma)$, which sets a stringent bound on the charged-Higgs mass [16]. The type-II 2HDM further permits the possibility of large down-type Yukawa couplings, a scenario motivated by the possibility of bottom-top Yukawa unification. Such large-$\tan\beta$ scenarios are efficiently constrained by $\mathcal{B}(B_s \to \mu^+\mu^-)$ [9, 17, 18] and we will come back to this topic in section 5. Concerning the first above-mentioned motivation, the Higgs sector of the MSSM is really richer than that of the type-II 2HDM: In the limit of infinitely heavy superpartners one encounters non-decoupling loop-induced Yukawa matrices $\epsilon^{u,d}$, an effect caused by the supersymmetry-breaking terms [19–21]. Despite the loop suppression large effects are possible in FCNC processes with down-type quarks which involve the product $\epsilon^d \tan\beta$ [22–27] with huge impact on $\mathcal{B}(B_s \to \mu^+\mu^-)$ [22–25, 28].

The phenomenological constraints from meson-antimeson mixing and rare (semi-)leptonic decays place severe bounds on the off-diagonal elements of ϵ^d, while those of ϵ^u are essentially unconstrained except for ϵ^u_{12} and ϵ^u_{21}. This situation calls for a variant of the 2HDM in which $Y^{u,d}$ and ϵ^u are arbitrary, while ϵ^d is suppressed. A strong motivation for such a model is the possibility of spontaneous CP violation, implemented through a Higgs potential developing complex vevs and real Yukawa matrices. Spontaneous CP violation is not possible with a 2HDM of type I or II, but requires at least three out of the four matrices in Eq. (3.9) to be non-zero. Avoiding fine-tuning implies that the better part of the needed effect stems from ϵ^u, while ϵ^d can be neglected [29]. However, in such a model, the mixing of the neutral Higgs fields is different from Eq. (3.19) and instead involves all three fields. Yet for the CP-conserving observables considered in this paper this feature is of minor relevance. The 2HDM scenario with sizable $Y^{u,d}$ and ϵ^u has the appealing feature that it simultaneously permits both measurable effects in FCNC processes *and* sufficiently light masses of the non-standard Higgs particles enabling their discovery at the LHC.

Setting ϵ^d naively to zero leads to a non-renormalisable model, because there are UV-divergent loops involving up-type quarks with $Y^{u,d}$ and ϵ^u couplings, which require counterterms proportional to elements of ϵ^d. Whenever one seeks to constrain the elements g^u_{jk} of Eq. (3.16) from FCNC transitions of down-type quarks, one must foresee such a counterterm to find a meaningful prediction. For example, $B_s \to \mu^+\mu^-$ is a $b \to s$ transition constraining g_{ct} and the corresponding loop contribution requires a counterterm for g_{sb}. The minimal renormalisable theory is found by invoking flavour symmetries and systematically expanding in terms of the spurions breaking these symmetries [30, 31]. The 2HDM gauge sector is invariant under unitary rotations $Q \to U_Q Q$, $d_R \to U_d d_R$, $u_R \to U_u u_R$ in flavour space with $(U_Q, U_d, U_u) \in SU(3)^3$ and the Yukawa sector is formally invariant under this flavour symmetry if one transforms the matrices in Eq. (3.9) as

$$Y^{u,d} \to U_Q Y^{u,d} U^\dagger_{u,d}, \qquad \epsilon^{u,d} \to U_Q \epsilon^{u,d} U^\dagger_{u,d}. \tag{3.20}$$

We propose to categorise the classes of renormalisable 2HDM in terms of the spurions breaking the $SU(3)^3$ flavour symmetry of the quark sector.[1] The minimal choice are two spurions, with just two physically distinct possibilities. Both comply with the definition of minimal flavour violation (MFV) as defined in Ref. [31]. The first possibility is to take $Y^{u,d}$

[1]The generalisation to the lepton sector is straightforward, but not relevant for the calculations in this paper.

as spurions and express the other two Yukawa matrices as $\epsilon^{u,d} = P_{u,d}(Y^u Y^{u\dagger}, Y^d Y^{d\dagger})\, Y^{u,d}$, where P_u and P_d are polynomials. This variant is discussed in Ref. [31] and amounts to a generalisation of the 2HDM of type II. It also constitutes a renormalisable extention of the aligned 2HDM of Ref. [32, 33], in which $P_{u,d}$ are constants. If the 2HDM is the low-energy limit of a more fundamental theory obeying the considered two-spurion symmetry-breaking pattern, the latter will naturally induce $\epsilon^{u,d}$ in the described way as well. An example for such a UV theory is the MSSM with a flavour-blind supersymmetry breaking mechanism (such as gauge mediation). The second possibility is to choose Y^d, ϵ^u as spurions, leading to a generalisation of the type-I 2HDM.

There are two possibilities for a 2HDM with three spurions, which can be taken as $Y^{u,d}$ plus either ϵ^u or ϵ^d. The first possibility is the phenomenologically interesting one and studied in this paper. The expansion up to third order reads

$$\begin{aligned} \epsilon^d = cY^d &+ c_{11} Y^d Y^{d\dagger} Y^d \\ &+ b_{11} \epsilon^u \epsilon^{u\dagger} Y^d + b_{12} \epsilon^u Y^{u\dagger} Y^d + b_{21} Y^u \epsilon^{u\dagger} Y^d + b_{22} Y^u Y^{u\dagger} Y^d \end{aligned} \tag{3.21}$$

with complex coefficients $c, \ldots, b_{22}$.

Concerning Eq. (3.21) several comments are in order:

- The spurion expansion is only meaningful, if the contributions to the off-diagonal elements of ϵ^d from higher electroweak orders (with five or more Yukawa matrices) are small, so that they can be neglected. A sufficient condition for this is realised in scenarios in which $c_{11}, \ldots, b_{22}$ are induced by one-loop contributions in either the UV completion or the 2HDM, while terms with $(2n+1)$ spurions are only generated at n-loop order and beyond. We consider this scenario throughout this paper.[2] Additional QCD corrections (e.g. an extra loop with a gluon) comply with the pattern in Eq. (3.21), i.e. QCD renormalises the coefficients, but does not induce new ones.

- By rotating $\left(H_u, H_d\right)$ in Eq. (3.9) one can eliminate c in Eq. (3.21). But in general radiative corrections bring this term back and a counterterm to c is needed, unless one corrects the rotation in each order of perturbation theory. It is therefore advisable to keep c in Eq. (3.21); we treat it as a perturbative quantity with $c = 0$ at tree level.

- The decay $B_s \to \mu^+\mu^-$ involves the FCNC vertex $\overline{Q}_j$-d_{Rk}-H_d with $(j,k) = (2,3)$. The dominant one-loop vertex diagram involves an internal H_d line and the product $Y^d Y^{d\dagger} Y^d$ or $\epsilon^u \epsilon^{u\dagger} Y^d$ stemming from the three H_d Yukawa couplings. The UV divergences can be cancelled by counterterms to c_{11} and b_{11}.

- With Eq. (3.12) we can trade $Y^{u,d}$ in Eq. (3.21) for the quark masses and CKM elements. Compared to the SM we find 14 additional complex parameters, the 9 entries of ϵ^u and $c_{11}, \ldots b_{22}$. Yet it is much more convenient to express observables

[2] A different application of Eq. (3.21), in which $c_{11}, \ldots, b_{22} = \mathcal{O}(1)$ is allowed, is the case that Y^u and ϵ^u are almost aligned, so that Eq. (3.12) means small off-diagonal matrix elements of these matrices in the chosen basis. Since $Y^u_{33}, \epsilon^u_{33} = \mathcal{O}(1)$ and further $Y^d_{33} = \mathcal{O}(1)$ is possible, some terms with five spurions must be added to Eq. (3.21), just as in the MFV case of Ref. [31].

in terms of g^u_{jk} of Eq. (3.16) instead of ϵ^u_{jk} and then use Eqs. (3.17) and (3.21) (with Eq. (3.12)) to calculate the g^d_{jk} in terms of the coefficients of the spurion expansion. While this procedure is needed in a global analysis of all available data —which is beyond the scope of this paper—, the study of $b \to s$ transitions alone will simply involve g_{ct} and g_{tt}.

In a practical calculation it is cumbersome to implement the renormalisation procedure in the described way, by providing counterterms to ϵ^u_{jk} and $c, \ldots, b_{22}$. Instead, it is much easier to renormalise the $g^{u,d}_{jk}$. If one renormalises all $g^{u,d}_{jk}$ in the $\overline{\text{MS}}$ scheme, one automatically complies with SU(2)×U(1) gauge symmetry. Therefore it is sufficient to choose the g^d_{jk} in such a way that Eq. (3.21) is obeyed at tree level. In our calculation we will only need a counterterm to g_{sb} (in addition to the usual QCD counterterms for the SM parameters), if m_s is set to zero. If m_s is kept, one finds primed Wilson coefficients which require a counterterm to g_{bs}.

4 Computational setup

In this section, we describe the chain of programs used to generate and evaluate the corresponding Feynman diagrams at leading and next-to-leading order. We use `FeynRules` with the `Universal FeynRules Output` (`UFO`) [34–36] to obtain Feynman rules for the model. The output is processed by `tapir` [37] into a Lagrangian file, which is used with `qgraf` [38] in order to generate all Feynman diagrams.

We compute the one-loop diagrams for general electroweak gauge parameters for the W and Z bosons and check that they drop out in the final result. This is a welcome check for the conversion from `UFO` to `qgraf` and `tapir`. If diagrams with all different quark flavours are explicitly calculated, we have at one-loop level $< \mathcal{O}(100)$ Feynman diagrams in the SM,[3] and an additional $\mathcal{O}(300)$ diagrams from contributions with at least one non-SM Higgs boson, most of which are Higgs-penguin diagrams.

At two loop-order, we perform the calculation in the Feynman gauge for the W and Z bosons. The diagrams are then converted with the help of `tapir` into `FORM` [39] code using Feynman rule definitions that were also produced in the conversion from `UFO` to the `qgraf` Lagrangian file. The individual expressions for the diagrams are mapped onto integral families using `exp` [40, 41] and a custom `FORM` setup is used to perform the remaining computational steps. Since the Wilson coefficients are independent of the momenta of the external particles, we set the latter to zero, so that only vacuum integrals need to be computed. (An exception are diagrams with an FCNC self-energy in an external leg, which are calculated with on-shell b quark and $m_b \neq 0$ before the subsequent limit $m_b \to 0$ is taken.) We use a `FORM` implementation of the algorithm presented in Ref. [42], see Ref. [43].

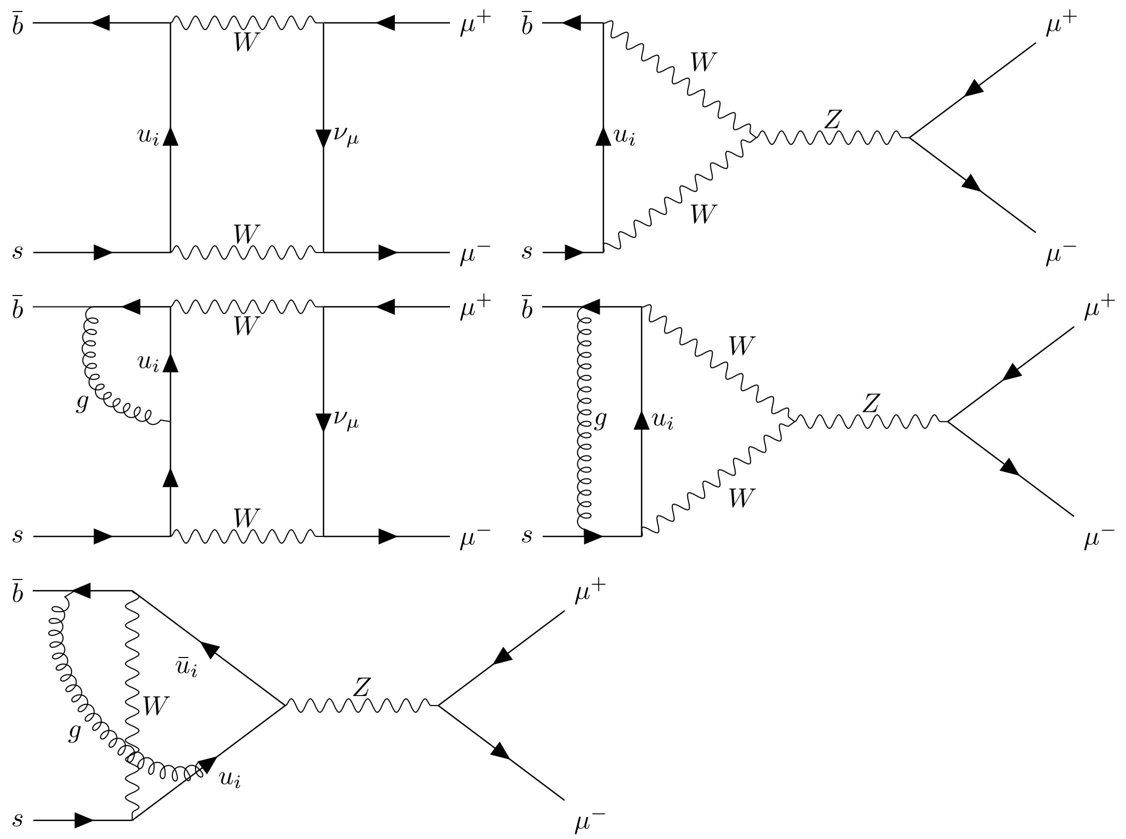

Figure 1. Sample diagrams contributing to C_A at leading and next-to-leading order in the SM.

5 The decay $\mathrm{B_s} \to \mu^+\mu^-$ in the Two-Higgs-Doublet Model of type-II

In the SM next-to-leading order corrections are available from Refs. [44–48] and higher order QCD and electroweak corrections have been computed in Refs. [9, 10, 18, 49, 50]. Next-to-leading corrections in the type-II 2HDM have been computed in Refs. [17, 51–53], which we have reproduced for the present paper, also as a check of the automated setup. The result can be expressed in terms of dimensionless mass ratios of the top quark, W boson and charged Higgs boson masses,

$$x_t = \frac{m_t^2}{M_W^2}\,, \qquad\qquad r_H = \frac{m_t^2}{M_{H^+}^2}\,. \tag{5.1}$$

In the SM, only the Wilson coefficient C_A receives significant contributions from diagrams such as the ones depicted in Fig. 1. The Wilson coefficients $C'_A, C_S, \ldots, C'_P$ are suppressed by powers of ratios of light (external) masses and M_W. The leading SM contribution is, moreover, independent of the Yukawa couplings of all external particles, that is we can set

[3] From the technical perspective, it is convenient to split the electroweak gauge bosons into two different "particles", with different propagator denominators $\left(k^2 - M^2\right)^{-1}$ and $\left(k^2 - \xi M^2\right)^{-1}$, respectively, and treat them as different diagrams; hence the large number of diagrams in the 1-loop calculation.

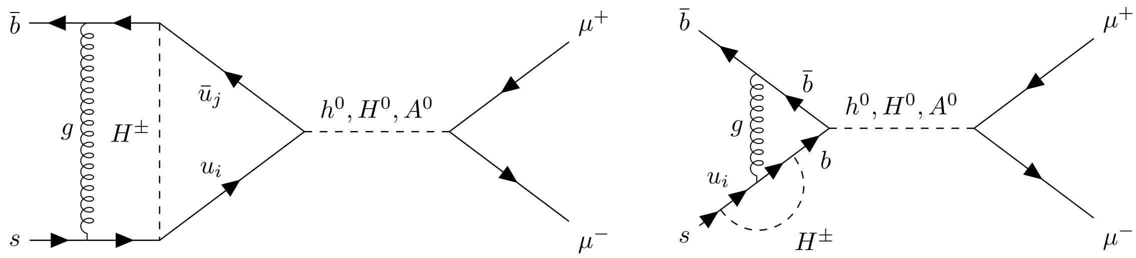

Figure 2. Sample two-loop Feynman diagrams contributing to the Wilson coefficients $C_S^{(\prime)}$ $(H_{1,2})$ and $C_P^{(\prime)}$ (A^0). In the left diagram, only flavour-diagonal transitions $i = j$ are possible in the type-II 2HDM, while the more general 2HDM allows also for transitions with $i \neq j$, e.g. transitions from a charm quark into a top quark.

$m_b = m_s = m_\mu = 0$ for the contributions from W-box and Z-penguin diagrams. At leading and next-to-leading order they are given by

$$C_A^{W+Z,(0)} = \frac{x_t\,(x_t-4)}{8\,(x_t-1)} + \frac{3x_t^2\log x_t}{8\,(x_t-1)^2}\,, \tag{5.2}$$

$$\begin{aligned} C_A^{W+Z,(1)} = & \frac{2x_t\left(2x_t^2+5x_t+5\right)}{3\,(x_t-1)^2} - \frac{x_t\left(x_t^2+5x_t+2\right)\log x_t}{(x_t-1)^3} - \frac{x_t\left(x_t^2+2\right)\mathrm{Li}_2\left(1-\frac{1}{x_t}\right)}{(x_t-1)^2} \\ & + \left(\frac{x_t\left(x_t^2+x_t+4\right)}{(x_t-1)^2} - \frac{6x_t^2\log x_t}{(x_t-1)^3}\right)\log\frac{\mu^2}{m_t^2}\,, \end{aligned} \tag{5.3}$$

where the Z-penguin contributions include the flavour-changing quark self-energy diagrams required to make the penguin diagrams finite. Moreover, since charm and up quark masses can be neglected compared to M_W and m_t, after summation over internal up-type quarks all contributions are proportional to the CKM factor $V_{ts}V_{tb}^*$ (contained in the normalisation factor N defined in Eq. (2.3)) due to the unitarity of the CKM matrix.

In the type-II Two-Higgs-Doublet model, the leading terms are given by $\mathcal{O}\left(\tan^2\beta\right)$ contributions to $C_S^{(\prime)}$ and $C_P^{(\prime)}$, arising from penguin diagrams with a neutral Higgs boson, see e.g. Fig. 2, and the W^+-H^+ box diagram. The Higgs-penguin contributions to C_S are given by

$$C_S^{h,(0)} = -\,r_b\left[\frac{r_H x_t\log r_H}{4\,(r_H-1)\,(r_H-x_t)} - \frac{r_H x_t\log x_t}{4\,(x_t-1)\,(r_H-x_t)}\right]\,, \tag{5.4}$$

$$\begin{aligned} C_S^{h,(1)} = -\,r_b\Bigg[& -\frac{8r_H x_t}{3\,(r_H-1)\,(x_t-1)} + \frac{2r_H x_t\,(3r_H-7)\log r_H}{3\,(r_H-1)^2\,(r_H-x_t)} - \frac{2r_H x_t\,(3x_t-7)\log x_t}{3\,(x_t-1)^2\,(r_H-x_t)} \\ & - 2\log\left(\frac{\mu^2}{m_t^2}\right)\left(\frac{r_H x_t}{(r_H-1)\,(x_t-1)} + \frac{r_H x_t\log r_H}{(r_H-1)^2\,(r_H-x_t)} - \frac{r_H x_t\log x_t}{(x_t-1)^2\,(r_H-x_t)}\right) \\ & + \frac{2r_H x_t\mathrm{Li}_2\left(1-\frac{1}{r_H}\right)}{r_H-x_t} - \frac{2r_H x_t\mathrm{Li}_2\left(1-\frac{1}{x_t}\right)}{r_H-x_t}\Bigg]\,, \end{aligned} \tag{5.5}$$

where

$$r_q = \frac{m_\mu m_q \tan^2\beta}{M_W^2} \,. \tag{5.6}$$

The Wilson coefficients for the right-handed operators $C_S^{\prime h,(i)}$ can be obtained by the replacement $r_b \to r_s$ in Eqs. (5.4) and (5.5). Further contributions include terms of order $m_b m_s m_\mu^2 \tan^4\beta/M_W^4$ and $m_t^2 m_\mu^2/M_W^4$ entering the Wilson coefficients C_A' and C_A, respectively, as well as $\mathcal{O}\left(m_b m_s \tan^2\beta/M_W^2\right)$ (in C_A') and $\mathcal{O}\left(m_t^2 \cot^2\beta/M_W^2\right)$ (in C_A) terms arising from Z-penguin diagrams with a charged Higgs boson. Box diagrams with a single charged Higgs boson also contribute to $C_{S,P}$ ($C'_{S,P}$), with Wilson coefficients proportional to m_b (m_s). We do not explicitly list these contributions here; they can be found in Refs. [51–53]. With the exception of the doubly muon-mass suppressed H^+–H^- box contributions to C_A, we include all of these additional terms in our analysis. The feature that C_S and C_P are proportional to m_b while their primed counterparts are proportional to m_s holds beyond the type-II 2HDM in our more general 2HDM with three spurions because of $\epsilon^d = P_d\left(\epsilon^u, Y^u, Y^d\right) Y^d$, entailing factors of m_{d_j} in Yukawa couplings of d_{jR}. A rather remarkable feature of the type-II 2HDM is the fact that the leading terms in $\tan\beta$ depend only on $\tan\beta$ and the charged-Higgs boson mass M_{H^+}, that is they are independent of the parameters of the neutral Higgs sector [17]. In the type-II 2HDM, the leading $\tan^2\beta$ contributions to the pseudoscalar and scalar Wilson coefficients satisfy the rather simple relation

$$C_S = C_P \,, \qquad C_S' = -C_P' \,. \tag{5.7}$$

In Fig. 3 we show the branching ratio $\mathcal{B}\left(B_s \to \mu^+\mu^-\right)$ in the type-II 2HDM as a function of the charged Higgs boson mass. The horizontal gray, blue, and violet bands correspond to the experimental measurements of LHCb [57] and CMS [56] as well as the theory prediction [18], respectively, including 2σ uncertainties for the experimental values (cf. Table. 1). The theory prediction of Ref. [18] uses $|V_{cb}| = 0.0424 \pm 0.0009$, which is close to today's value inferred from inclusive $b \to c\ell\nu$ decays. If one uses $|V_{cb}| = 0.03936 \pm 0.00068$ from exclusive B decays [58] the central value of the theory prediction for $10^9\mathcal{B}\left(B_s \to \mu^+\mu^-\right)$ drops from 3.65 to 3.15.

The coloured lines are predictions from the 2HDM for different values of $\tan\beta$. It is interesting to note that for $\tan\beta = 25$ low values of $M_{H^\pm}$ are required to reproduce the central value of the LHCb measurement. Recently it has been pointed out that LHC data still permit $M_{H^\pm} \leq 400\,\text{GeV}$ with couplings compatible with solutions of the $b \to c\tau\nu$ flavour anomalies [59]. Charged-Higgs explanations of the latter have been found viable in Ref. [60, 61] and are invigorated by recent LHCb data on $B \to D^{(*)}\tau\nu$ [62], see Refs. [63, 64]. Of course, in the limit $M_{H^\pm} \to \infty$ all 2HDM curves approach the SM prediction. Note that in the type-II model there is a $\tan\beta$-independent 95% C.L. lower bound on $M_{H^\pm}$ in the range 570-800 GeV from $B \to X_s\gamma$ [16]. This bound can be easily weakened with our model's additional couplings discussed in the following section. While charged Higgs searches at the LHC are compatible with the quoted $H^\pm$ masses [65], the lower bound on $M_{H^\pm}$ inferred from the data on $gg/b\bar{b} \to A^0[\to \tau^+\tau^-]$ searches is larger than 1 TeV [66] in

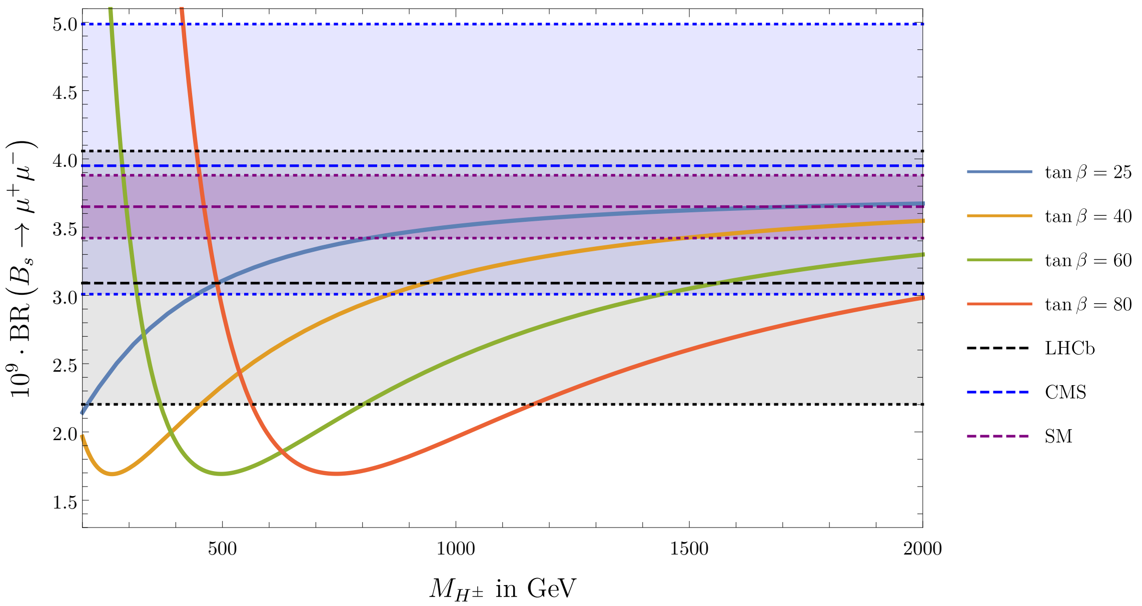

Figure 3. Branching ratio $\mathcal{B}\left(B_s \to \mu^+\mu^-\right)$ in the type-II Two-Higgs-Doublet model at next-to-leading order in QCD, for different values of $\tan\beta$. All running parameters are evaluated at the scale $\mu = \overline{m}_t\left(\overline{m}_t\right)$. The black dashed and dotted lines denote the central value and the experimental 2σ error of the LHCb measurement [54, 55], respectively, the blue band shows the corresponding information for the CMS result [56]. The purple dashed and dotted bands indicate the SM prediction with uncertainties, presented in Ref. [18]. Note that the SM predictions in the purple band were obtained including also $\mathcal{O}\left(\alpha_s^2\right)$ and $\mathcal{O}\left(\alpha_{\mathrm{em}}\right)$ contributions.

perturbed versions of the type-II 2HDM, but can be weakened if e.g. the A^0 coupling to τ's is modified w.r.t. to the type-II form in Eq. (3.18).

6 Additional contributions in a model with flavour-changing neutral Yukawa couplings

In a model with a Yukawa Lagrangian given by Eq. (3.16) there are additional tree-level contributions $\bar{b}s \to h^0(H^0, A^0) \to \mu^+\mu^-$ of order $\tan\beta$. A sample Feynman diagrams is shown in Fig. 4. At loop-level there are $\mathcal{O}(\tan^3\beta)$ terms due to diagrams in which the neutral Higgs boson couples to the b line. At LO these are diagrams with a FCNC self-energy and we also refer to them as self-energy diagrams at NLO, even if a gluon connects the FCNC loop with the s quark as in the diagram on the right in Fig. 2. These $\mathcal{O}\left(\tan^3\beta\right)$ terms occur because a $\tan\beta$-enhanced coupling in the self-energy diagrams is not cancelled by a factor $\cot\beta$ in the second charged-Higgs coupling, which is a distinguishing feature compared to the type-II model. If these self-energy diagrams involve a helicity flip of the internal fermion line, see Fig. 5, they come with a factor of $\tan\beta$ and are linear in the flavour-changing Yukawa matrix $\hat{g}^u$, which enters the result through the charged-Higgs coupling in the fourth term of Eq. (3.16). In fact, the dominant dependence on g_{ct} stems from this source and not from diagrams in which a neutral Higgs boson couples to charm

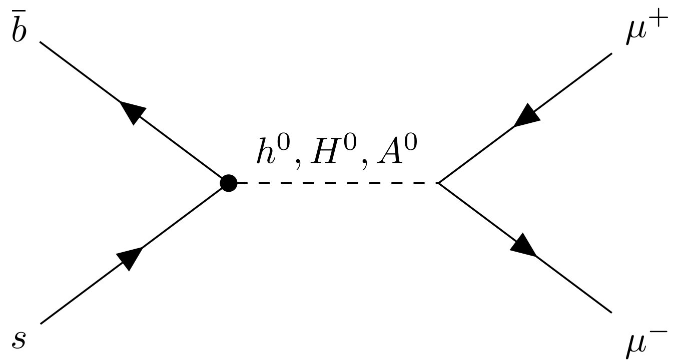

Figure 4. Tree-level diagrams with flavour-changing neutral Higgs couplings. The $b - s - H$ coupling is denoted by a dot on the vertex.

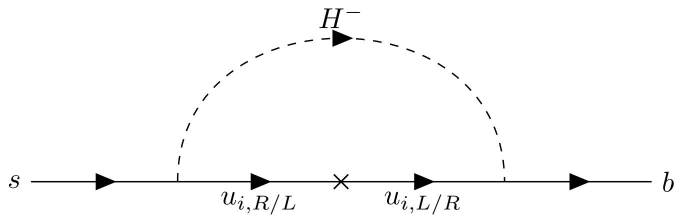

Figure 5. The loop-induced change of flavours $s \to b$ via a quark self-energy diagram. The helicity flip denoted by the cross ensures a factor of $\tan\beta$ and linearity in $\hat{g}^u$.

---

and top in a vertex diagram, which have a factor of $\tan\beta$ less. Note that contributions from diagrams without helicity flip are either already included in the type-II model or quadratic in $\hat{g}^u$ (and without the factor $\tan\beta$), and we will consequently neglect the latter in what follows.

6.1 Pseudoscalar Wilson coefficient C_P

At tree level the Wilson coefficient C_P originating from the diagram in Fig. 4 with a virtual A^0 boson is given by

$$C_P^{(0),\text{tree}} = -\frac{\pi^2}{G_F^2 M_W^2 V_{tb}^* V_{ts}} \frac{m_\mu \tan\beta}{2v M_{A^0}^2} g_{sb}^* = -\frac{g_{sb}^*}{g_{bs}} C_P^{\prime(0)} . \tag{6.1}$$

Since there is no loop-suppression, even small values of g_{bs} and g_{sb}^* can have significant impact on the branching ratio, but the spurion expansion in Eq. (3.21) naturally leads to (parametrically suppressed) small couplings. For convenience, let us define the linear combinations $g_{bs}^{\pm} \equiv g_{bs} \pm g_{sb}^*$.

At one-loop order only the self-energy diagrams contain an enhancement factor $\tan^3\beta$ whereas the vertex contributions contain at most a quadratic term. The one-loop self-energy contributions to C_P and C_P' are ultra-violet divergent. The corresponding counterterm is generated from Eq. (6.1) and is of the form

$$g_{bs}^{+,0} = g_{bs}^{+} + \delta_{A^0,bs}^{(0)} + \left(\frac{\alpha_s}{4\pi}\right) \delta_{A^0,bs}^{(1)} + \dots . \tag{6.2}$$

In the $\overline{\text{MS}}$ renormalisation scheme the one-loop contribution is given by

$$\delta^{(0)}_{A^0,bs} = -\frac{1}{\epsilon}\frac{\sqrt{2}G_F m_t \tan^2\beta}{8\pi^2}\left[m_s g_{ct} V_{ts} V^*_{cb} + \left(m_s g_{tt} V_{ts} + m_b g^*_{ct} V_{cs} + m_b g^*_{tt} V_{ts}\right) V^*_{tb}\right] . \tag{6.3}$$

Here, the terms with m_b renormalise the Wilson coefficient C_P, while the ones with m_s renormalise the Wilson coefficient C'_P. The renormalised finite pseudoscalar Wilson coefficients read

$$\begin{aligned} C_P^{(0)} &= C_P^{(0),\text{tree}} + \tilde{N}\,\frac{m_b}{M^2_{A^0}}\left(g^*_{ct}\frac{V_{cs}}{V_{ts}} + g^*_{tt}\right)\tilde{C}_P^{(0)} , \\ C_P^{\prime(0)} &= C_P^{\prime(0),\text{tree}} - \tilde{N}\,\frac{m_s}{M^2_{A^0}}\left(g_{ct}\frac{V^*_{cb}}{V^*_{tb}} + g_{tt}\right)\tilde{C}_P^{(0)} , \end{aligned} \tag{6.4}$$

with normalisation factor

$$\tilde{N} = \frac{m_t m_\mu \tan^3\beta}{G_F\sqrt{2}M_W^2 v} = \frac{g m_t m_\mu \tan^3\beta}{2G_F M_W^3}, \tag{6.5}$$

the weak coupling constant g, and

$$\tilde{C}_P^{(0)} = -\frac{1}{8}\left[1 + \log\left(\frac{\mu^2}{m_t^2}\right) - \frac{\log r_H}{r_H - 1}\right] . \tag{6.6}$$

At NLO in QCD (i.e. two-loop order), the counterterm required to obtain a finite result is given by

$$\begin{aligned} \delta^{(1)}_{A^0,sb} = &-\frac{G_F m_t \tan^2\beta}{\sqrt{2}\pi^2}\left[m_s g_{ct} V_{ts} V^*_{cb} + \left(m_s g_{tt} V_{ts} + m_b g^*_{ct} V_{cs} + m_b g^*_{tt} V_{ts}\right) V^*_{tb}\right] \\ &\times\left[\frac{1}{\epsilon^2} + \frac{4}{3\epsilon}\right] . \end{aligned} \tag{6.7}$$

Note that in addition to the top quark mass m_t also the flavour-changing Yukawa couplings are minimally renormalised. The two-loop contribution to the Wilson coefficients reads

$$\begin{aligned} C_P^{(1)} &= \tilde{N}\,\frac{m_b}{M^2_{A^0}}\left(g^*_{ct}\frac{V_{cs}}{V_{ts}} + g^*_{tt}\right)\tilde{C}_P^{(1)} , \\ C_P^{\prime(1)} &= -\,\tilde{N}\,\frac{m_s}{M^2_{A^0}}\left(g_{ct}\frac{V^*_{cb}}{V^*_{tb}} + g_{tt}\right)\tilde{C}_P^{(1)} , \end{aligned} \tag{6.8}$$

with

$$\begin{aligned} \tilde{C}_P^{(1)} = &-\frac{4(r_H-2)}{3(r_H-1)} + \frac{(3r_H-7)\log(r_H)}{3(r_H-1)^2} + \left(\frac{7-4r_H}{3(r_H-1)} - \frac{\log(r_H)}{(r_H-1)^2}\right)\log\left(\frac{\mu^2}{m_t^2}\right) \\ &-\frac{1}{2}\log^2\left(\frac{\mu^2}{m_t^2}\right) + \mathrm{Li}_2\left(1 - \frac{1}{r_H}\right) . \end{aligned} \tag{6.9}$$

6.2 Scalar Wilson coefficient C_S

The scalar Wilson coefficients receives contributions from both neutral CP-even Higgs mass eigenstates h^0 and H^0. At tree level, the diagrams with h^0 and H^0 give rise to the Wilson coefficients

$$C_S^{(0),\text{tree}} = -\frac{\pi^2}{G_F^2 M_W^2 V^*_{tb} V_{ts}}\frac{m_\mu \tan\beta}{2v} R_M g^*_{sb} = \frac{g^*_{sb}}{g_{bs}} C_S^{\prime(0)} , \tag{6.10}$$

where

$$R_M = \frac{M_{h^0}^2 \sin^2(\beta - \alpha) + M_{H^0}^2 \cos^2(\beta - \alpha)}{M_{h^0}^2 M_{H^0}^2} \tag{6.11}$$

contains the dependence on the neutral Higgs-boson masses. The counterterms required to cure the divergences at one and two loops can be obtained from Eqs. (6.3) and (6.7) by the simple replacements $g_{ct} \to -g_{ct}$ and $g_{tt} \to -g_{tt}$. The renormalised Wilson coefficients C_S and C_S' are related to the pseudoscalar ones by

$$C_S^{(i)} = \frac{R_M}{M_{A^0}^2} C_P^{(i)}, \qquad C_S'^{(i)} = -\frac{R_M}{M_{A^0}^2} C_P'^{(i)}. \tag{6.12}$$

Note that there are no QCD corrections to $C_{S,P}^{(\prime),\text{tree}}$ since they cancel in the matching calculation.

7 Phenomenology

In this section we discuss the possible size of $\mathcal{B}(B_s \to \mu^+\mu^-)$ in our 2HDM under the constraint that other $b \to s$ processes comply with the data. We include the tree-level contributions from diagrams with flavour-changing down-type couplings (cf. Fig. 4), as well as the SM results and the leading quadratic $\tan\beta$ contributions in the type-II 2HDM to which the additional diagrams of order $\tan^3\beta$ discussed in the previous section add as corrections.

In a generic 2HDM the tree-level couplings $g_{bs}^{\pm}$ will drastically increase the branching ratio for $B_s \to \mu^+\mu^-$ due to the missing loop suppression. In our model the spurion expansion suppresses $g_{bs}^{\pm}$ in a controlled way, but still permits large enough contributions to get phenomenologically interesting effects in $B_s \to \mu^+\mu^-$: Even rather small up-type couplings g_{ct} significantly modify the Wilson coefficients $C_P^{(\prime)}$ and $C_S^{(\prime)}$, as they feature a CKM factor V_{cs} instead of V_{ts}. In the following, we will restrict ourselves to the experimentally favoured scenario [67, 68] of aligned Higgs doublets, in which $\sin(\beta - \alpha) \approx 1$. For the numerical analysis, we will set $\sin(\beta - \alpha) = 1$, and therefore have $R_M = M_{H^0}^{-2}$. In this case, the Higgs mass eigenstates h^0 and H^0 coincide with ϕ^0 and $-\phi^{0\prime}$, respectively, and only the latter possesses non-SM-like couplings to fermions. This reduces the number of relevant non-Yukawa-type parameters of the extended Higgs sector to four, namely $\tan\beta$, M_{H^+}, M_{A^0} and $M_{\phi^{0\prime}} \equiv M_{H^0}$.

7.1 Constraints from $\mathbf{b \to s\gamma}$ decays

An important constraint on the magnitude of flavour-changing Yukawa couplings in the up-type quark sector arises from the inclusive rare decays $B \to X_s\gamma$. This process is mediated at the quark level by $b \to s\gamma$ through a top quark loop with a charged W boson in the Standard Model and receives additional contributions through charged-Higgs boson diagrams in the 2HDM, see Fig. 6. In order to eliminate the dependence on $V_{cb} \simeq -V_{ts}$, one traditionally works with the quantity

$$R_\gamma \equiv \frac{\mathcal{B}(b \to s\gamma) + \mathcal{B}(b \to d\gamma)}{\mathcal{B}(b \to cl\nu)}. \tag{7.1}$$

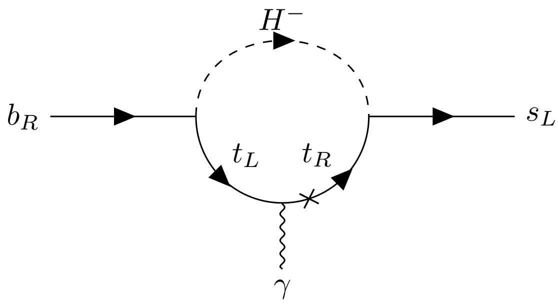

Figure 6. Sample Feynman diagram for the rare decay $b \to s\gamma$ at one loop in the 2HDM. The cross indicates a chirality flip $t_L \to t_R$.

Note that in the SM and the type-II 2HDM the branching ratio of $b \to d\gamma$ is much smaller than that of $b \to s\gamma$.

In the type-II 2HDM, the contribution of the charged Higgs diagrams to the decay rate is positive, moving the theoretical prediction for the branching ratio away from the experimental value averaged in [16] to

$$R_{\gamma,\text{exp.}} = (3.22 \pm 0.15) \cdot 10^{-3}\,, \tag{7.2}$$

where a lower cutoff of $E_0 \geq 1.6\,\text{GeV}$ has been put on the photon energy. The practical independence of R_γ of $\tan\beta$ in the largest part of the parameter space in the type-II 2HDM allowed for the extraction of a lower limit on the mass of the charged Higgs boson in [16], see section 5. In the general 2HDM, where the factor $\tan\beta$ from the btH^- vertex need not be cancelled by a factor $\cot\beta$ from the stH^- vertex, the quantity R_γ depends on $\tan\beta$. The combination of the $\bar{t}_L b_R H^+$ and $\bar{s}_L t_R H^-$ Yukawa couplings arising in the process is then given by

$$\left(\frac{m_b \tan\beta\, V_{tb}}{v}\right)\left(\frac{m_t\, V_{ts}^*}{v\tan\beta} + V_{ts}^*\, g_{tt} + V_{cs}^*\, g_{ct}\right) = \frac{m_b m_t\, V_{tb} V_{ts}^*}{v^2}\left(1 + g_{st}^{\text{eff}}\right)\,, \tag{7.3}$$

where we have defined the short-hand notation

$$g_{st}^{\text{eff}} \equiv \frac{v\,\tan\beta}{m_t}\left(g_{ct}\frac{V_{cs}^*}{V_{ts}^*} + g_{tt}\right)\,. \tag{7.4}$$

Note that g_{st}^{eff} carries a factor of $\tan\beta$. We stress that the limit $g_{st}^{\text{eff}} = 0$ corresponds to the type-II 2HDM, while the case $g_{st}^{\text{eff}} = -1$ is the Standard Model limit. In order to constrain our new flavour-changing couplings, we use the results from [69] and [16] with this trivial change of the $\bar{s}_L t_R H^-$ Yukawa coupling.

For large enough values of $M_{H^\pm}$, the central value of R_γ is approximately given (at

$\mu = \overline{m}_t(\overline{m}_t)$) by

$$R_\gamma \approx 10^{-4} \cdot \Bigg\{ 33.10|_{\rm SM} + \left(1 + \,{\rm Re}\, g_{st}^{\rm eff}\right) \Big[r_H \Big(-48.93 - 47.60 \log r_H - 0.99 \left(\log r_H\right)^2 - 0.15 \left(\log r_H\right)^3 + 4.71\, {\rm Li}_2 \left(1 - \frac{1}{r_H}\right)\Big) + r_H^2 \left(-53.82 - 98.18 \log r_H + 4.79\, {\rm Li}_2 \left(1 - \frac{1}{r_H}\right)\right) + r_H^3 \left(-56.04 - 150.43 \log r_H + 3.17\, {\rm Li}_2 \left(1 - \frac{1}{r_H}\right)\right)\Big] \Bigg\}, \quad (7.5)$$

which agrees with the exact result within 1 % in the complete subdomain of $\left(M_{H^\pm}, {\rm Re}\, g_{st}^{\rm eff}\right) \in [500\,{\rm GeV}, \infty) \times [-5, 5]$ in which R_γ lies within the band allowed by the experimental and theoretical uncertainties (see below). The approximate formula in Eq. (7.5) only includes the interference of the new-physics contribution with the SM result and neglects the squared new-physics contribution. In deriving Eq. (7.5) we have used Eq. (10) of Ref. [70]. We adopt the estimate of the theoretical uncertainty of about 6.73 % given in [16], consisting of individual uncertainties of 5 % (non-perturbative), 1.5 % (parametric), 3 % (higher-order), and 3 % (interpolation in the charm quark mass m_c). In Fig. 7, we illustrate the ratio R_γ in the $\left(M_{H^\pm}, {\rm Re}\, g_{st}^{\rm eff}\right)$ plane. The thick dashed line corresponds to the central experimental value in Eq. (7.2) and $R_{\gamma,{\rm exp}} \pm \Delta_{\rm exp+th}$, where $\Delta_{\rm exp+th} = 2\sigma_{\rm exp} + \delta_{\rm th}$ is the sum of the experimental 2σ uncertainty intervals and the theoretical uncertainty of 6.73 %. For small values of $M_{H^\pm}$, the allowed range of $g_{st}^{\rm eff}$ is tightly constrained around $g_{st}^{\rm eff} = -1$, due to the closeness of the Standard Model prediction and the experimental central value. At larger $M_{H^\pm}$, a significantly wider range of flavour-changing Yukawa couplings is allowed. From R_γ we derive $M_{H^\pm}$-dependent upper and lower bounds on Re $\left(g_{st}^{\rm eff}\right)$ which we will use in order to constrain the real part of the flavour-changing up-type couplings appearing in $B_s \to \mu^+\mu^-$.

7.2 Higgs searches

Searches for heavy Higgs bosons at the LHC put powerful lower limits on the masses of new Higgs particles, but these depend on the Yukawa sector of the considered 2HDM. For the case of the type-II model (or ramifications of it) these searches already exclude a significant portion of the $M_{A^0} - \tan\beta$ plane at present. In Fig. 8, we show a recent collection of exclusion limits obtained through various different searches by the ATLAS experiment [66] in a modification of the type-II model. These limits imply that large values of $\tan\beta$ can only be realised if at the same time the additional Higgs bosons are quite heavy, $M_{A^0} \gtrsim 1.5\,{\rm TeV}$.

It should be noted that for heavy M_{A^0} these bounds also approximately apply for M_{H^+} and M_{H^0}, since the masses become degenerate in the heavy-Higgs limit (for a thorough analysis of the allowed mass splittings see [71]). Note that the bounds from neutral Higgs searches are more constraining than those for H^+ searches [65]. The most stringent constraints are from final states with τ's and also apply to our lepton Yukawa Lagrangian in

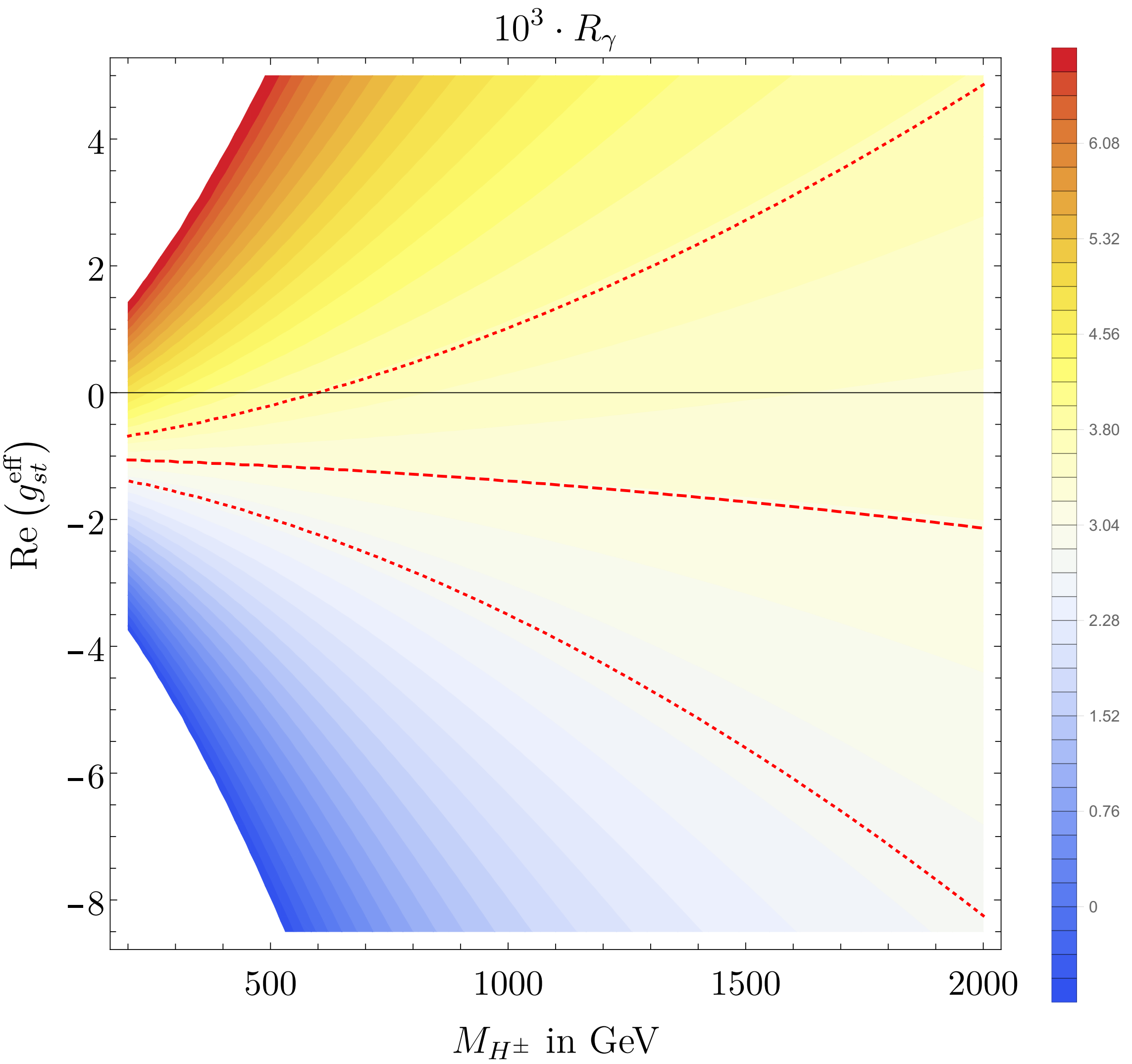

Figure 7. The ratio R_γ as a function of the charged Higgs boson mass $M_{H^\pm}$ and $g_{st}^{\rm eff}$. The dashed lines correspond to the experimental central value and the $\pm 2\sigma$ intervals, to which we have also added the theoretical uncertainties.

Eq. (3.18) which we have chosen of type-II. (However, the choice of the τ Yukawa couplings is of no relevance for the phenomenology of the $b \to s$ FCNC processes discussed in this paper.) The presence of the additional couplings g_{jk}^u will increase some branching ratios at the expense of those of decays into τ's, so that these bounds can be somewhat weakened, but the general trend remains valid. Our scenarios discussed below comply with the ATLAS bounds.

7.3 $\mathbf{B_s - \bar{B}_s}$ mixing

The effective $\bar{s}_L b_R A^0$ and $\bar{s}_L b_R H^0$ vertices are the sum of the tree-level couplings $\propto g_{sb}$ and the loop contributions involving vertex and self-energy diagrams $\propto g_{ct} V_{tb} V_{cs}^* + g_{tt} V_{tb} V_{ts}^*$. C_P

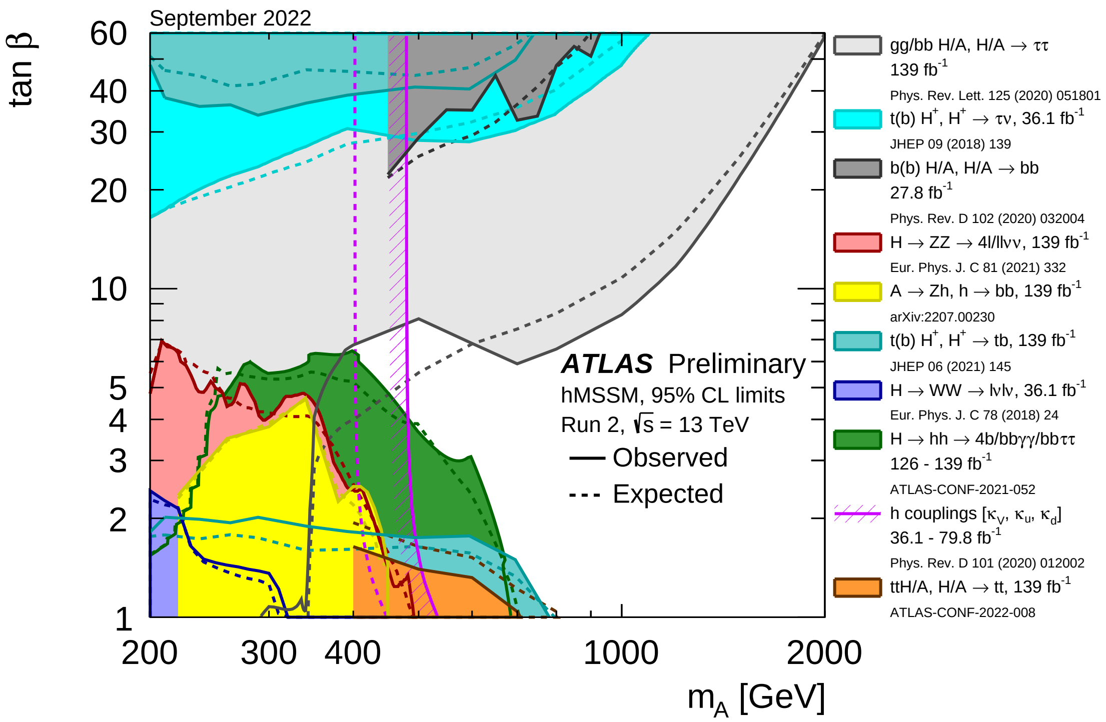

Figure 8. Exclusion limits in the $M_{A^0} - \tan\beta$ plane from different searches performed by the ATLAS experiment. Taken from [66]. The shown limits are for a different variant of the type-II 2HDM than ours, but qualitatively apply as well to our model.

and C_S are proportional to this effective vertex, which is therefore the relevant quantity constrained by $\mathcal{B}(B_s \to \mu^+\mu^-)$. Now the $B_s - \bar{B}_s$ mixing amplitude depends quadratically on this effective vertex, while both quantities drop quadratically with M_{A^0} and M_{H^0}, so that the quantities give complementary information on the parameter space. $B_s - \bar{B}_s$ mixing is mediated in the Standard Model by the $\Delta B = 2$ operator $Q_{VLL} = (\bar{b}_L \gamma_\mu s_L)(\bar{b}_L \gamma^\mu s_L)$ and in the 2HDM by three additional effective operators

$$\begin{aligned} Q_{SLL} &= (\bar{b}_R s_L)(\bar{b}_R s_L) \,, \\ Q_{SLR} &= (\bar{b}_R s_L)(\bar{b}_L s_R) \,, \\ Q_{SRR} &= (\bar{b}_L s_R)(\bar{b}_L s_R) \,, \end{aligned} \tag{7.6}$$

The Wilson coefficient of Q_{SLL}only involves the effective vertex governing $B_s \to \mu^+\mu^-$ and the tree-level propagators of A^0 and H^0, while the coefficients of the other operators also involve the corresponding chirality-flipped effective $\bar{s}_R b_L A^0$ and $\bar{s}_R b_L H^0$ vertices. The coefficient C_{SLL} (C_{SRR}) is proportional to m_b^2 (m_s^2), while the coefficient C_{SLR} is proportional to $m_b m_s$; we therefore drop the operator Q_{SRR} in our analysis. However, considering the ATLAS constraints implying large masses M_{A^0,H^0}, $C_{SLL} \propto 1/M_{A^0}^2 - 1/M_{H^0}^2$ is heavily suppressed due to the small splitting of Higgs masses in the large-mass limit, and C_{SLR} becomes relevant. This feature results from the fact that Q_{SLL} violates hypercharge by two units of the Higgs hypercharge and the coefficient C_{SLL} is therefore suppressed by a factor of $v^2/M_{A^0}^2$ compared to C_{SLR} multiplying Q_{SLR} which conserves hypercharge and SU(2). As a consequence, C_{SLR} is more important than C_{SLL}. This feature has been widely studied in the context of the effective 2HDM emerging from integrating out superpartners in the MSSM [23–25, 27].

In the following we correlate $\mathcal{B}(B_s \to \mu^+\mu^-)$ with $\mathcal{B}(B \to X_s\gamma)$ and the $B_s - \bar{B}_s$ oscillation frequency ΔM_{B_s}, which is proportional to the magnitude of the $B_s - \bar{B}_s$ mixing amplitude. Only the effective $\bar{s}_L b_R A^0$ and $\bar{s}_L b_R H^0$ vertices are physical, by e.g. changing the renormalisation condition for g_{sb} we can shift pieces between g_{sb} and the renormlised loop. For simplicity, we set the tree-value of g_{sb} to zero, i.e. consider the case that this coupling is only generated radiatively. The only non-trivial Yukawa structure entering the considered observables is then g_{st}^{eff}.

In Fig. 9 and Fig. 10 we illustrate the dependence of the branching ratio $\mathcal{B}\left(B_s \to \mu^+\mu^-\right)$ on the flavour-changing Yukawa couplings for some exemplary numerical values. We choose to show our results separately for the LHCb [54, 55] and CMS [56] measurements, which lie on different sides of the SM prediction calculated with the $|V_{cb}|$ from inclusive decays. The interval allowed on the horizontal axis (the real part $\text{Re}\left(g_{st}^{\text{eff}}\right)$) is for each choice of Higgs masses determined by the range allowed by $b \to s\gamma$. Recall that g_{st}^{eff} carries a factor of $\tan\beta$, which needs to be taken into account if the bounds on g_{st}^{eff} were to be converted into direct bounds on g_{ct} and g_{tt}. A priori generic $\leq \mathcal{O}(0.1)$ values of g_{ct} could make g_{st}^{eff} in Eq. (7.4) as large as $\mathcal{O}(50)$. For the considered Higgs masses such large values of $|g_{st}^{\text{eff}}|$ are forbidden by $b \to s\gamma$ and the range for $\text{Im}\left(g_{\text{eff},bs\gamma}\right)$ shown on the y axis in plots (a) to (d) only serves the purpose to show the constraint from $\mathcal{B}\left(B_s \to \mu^+\mu^-\right)$. Low values for Higgs masses enforce small values for $\tan\beta$ from the LHC searches, but for these scenarios $b \to s\gamma$ forbids any measurable effect in $\mathcal{B}\left(B_s \to \mu^+\mu^-\right)$. This situation changes if one considers large values for $\tan\beta$ and the Higgs masses, because $\mathcal{B}\left(B_s \to \mu^+\mu^-\right)$ grows faster with $\tan\beta$ than $\mathcal{B}(B \to X_s\gamma)$, see plots (e) and (f). We find that in the considered scenarios the bounds from $\mathcal{B}(B \to X_s\gamma)$ are stronger than those from ΔM_{B_s}, which we always find in the band allowed by the current theoretical uncertainty. This situation changes if we go to even larger Higgs masses, permitting larger values of $|g_{st}^{\text{eff}}|$ in $\mathcal{B}(B \to X_s\gamma)$. The quadratic dependence of ΔM_{B_s} on g_{st}^{eff} makes ΔM_{B_s} a good probe of the parameter region in which both the Higgs masses and g_{st}^{eff} are large.

We do not study the case of sizable imaginary parts of the new FCNC couplings here. These imaginary parts impact CP asymmetries such as $A_{CP}^{\text{mix}}(B_s \to J/\psi\phi)$, which will be investigated in a follow-up paper. All numerical SM input parameters are given in Tab. 1. Note that we do not take into account uncertainties in the input parameters as the dependence of the branching ratio is much weaker than the dependence due to the variation of flavour-changing Yukawa couplings.

We stress here that the presented calculation equally applies to $B_d \to \mu^+\mu^-$ with the change $V_{ts} \to V_{td}$, but this is not true anymore when considering the constraint from $B_d - \bar{B}_d$ mixing because of the additional dependence on the light quark mass. Since m_d is negligibly small, the $B_d - \bar{B}_d$ mixing amplitude becomes insensitive to the effective $\bar{b}dA^0$ and $\bar{b}dH^0$ couplings.

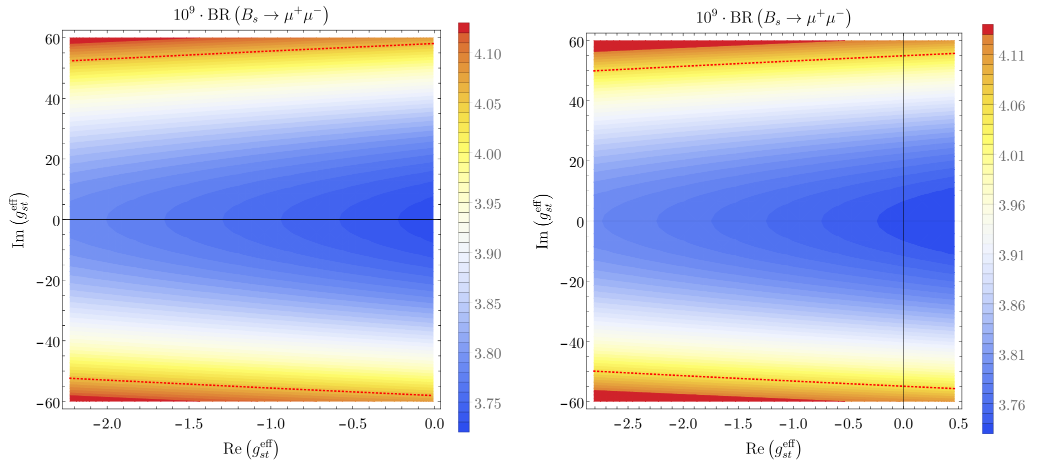

(a) $M_{H^\pm} = M_{H^0} = M_{A^0} = 600\,\mathrm{GeV}$, $\tan\beta = 7$.

(b) $M_{H^\pm} = M_{A^0} = 800\,\mathrm{GeV}$, $M_{H^0} = 600\,\mathrm{GeV}$, $\tan\beta = 7$.

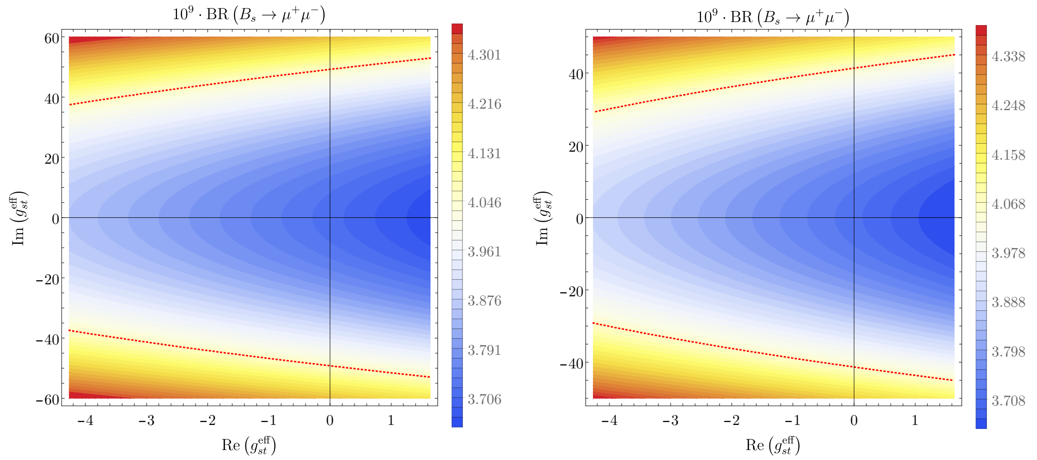

(c) $M_{H^\pm} = M_{H^0} = M_{A^0} = 1200\,\mathrm{GeV}$, $\tan\beta = 12$.

(d) $M_{H^\pm} = 1200\,\mathrm{GeV}$, $M_{H^0} = M_{A^0} = 1100\,\mathrm{GeV}$, $\tan\beta = 12$.

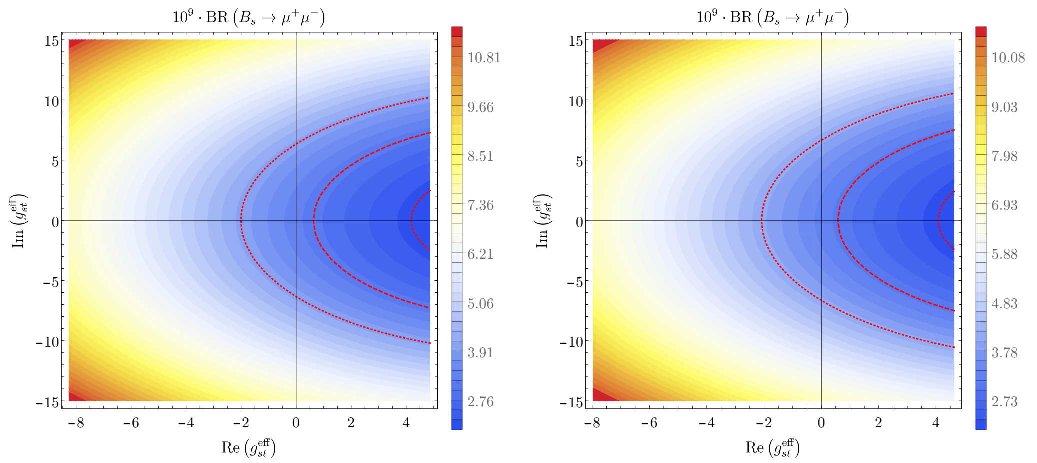

(e) $M_{H^\pm} = M_{H^0} = M_{A^0} = 2000\,\mathrm{GeV}$, $\tan\beta = 60$.

(f) $M_{H^\pm} = 1950\,\mathrm{GeV}$, $M_{H^0} = 2050\,\mathrm{GeV}$, $M_{A^0} = 2000\,\mathrm{GeV}$, $\tan\beta = 60$.

Figure 9. Branching ratio of $B_s \to \mu^+\mu^-$ for different values of Higgs masses and $\tan\beta$. All quantities are evaluated at $\mu = \overline{m}_t\,(\overline{m}_t)$. The red dashed and dotted lines indicate the experimental central value and the 2σ uncertainties of LHCb branching ratio measurement [54, 55], respectively. The constraint of $\mathcal{B}(B \to X_s\gamma)$ on $|\mathrm{Im}\, g_{st}^{\mathrm{eff}}|$ is not shown.

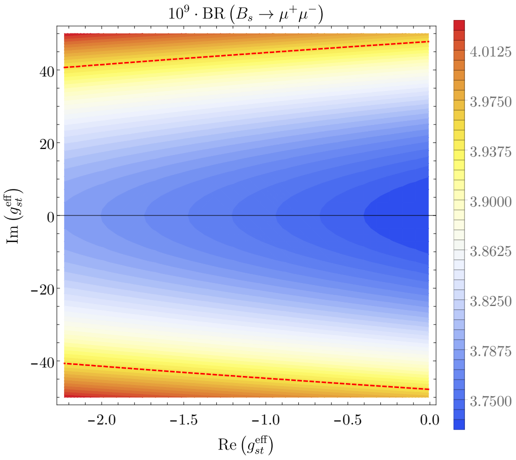

(a) $M_{H^\pm} = M_{H^0} = M_{A^0} = 600\,\mathrm{GeV}$, $\tan\beta = 7$.

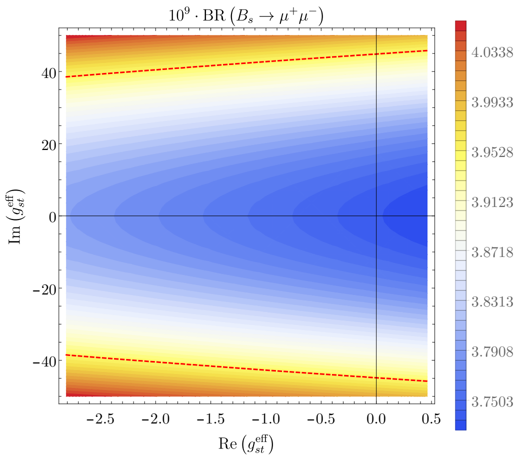

(b) $M_{H^\pm} = M_{A^0} = 800\,\mathrm{GeV}$, $M_{H^0} = 600\,\mathrm{GeV}$, $\tan\beta = 7$.

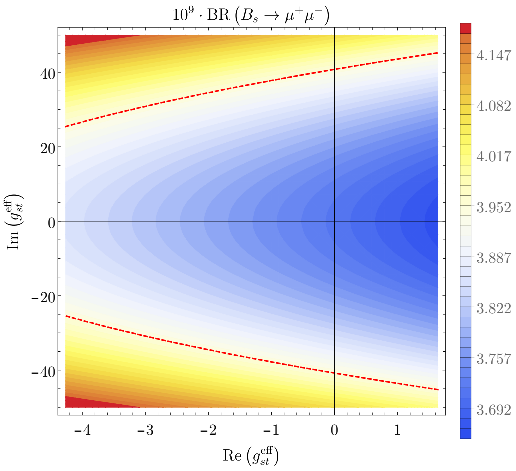

(c) $M_{H^\pm} = M_{H^0} = M_{A^0} = 1200\,\mathrm{GeV}$, $\tan\beta = 12$.

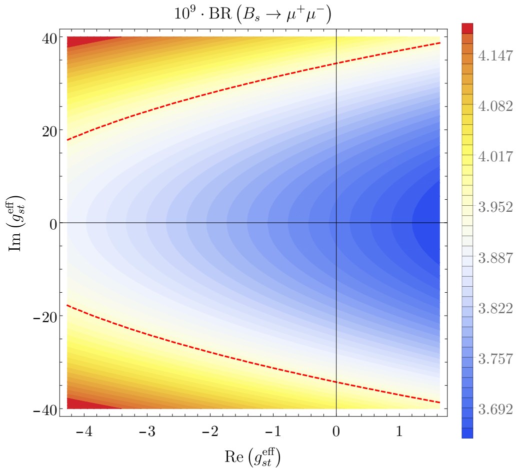

(d) $M_{H^\pm} = 1200\,\mathrm{GeV}$, $M_{H^0} = M_{A^0} = 1100\,\mathrm{GeV}$, $\tan\beta = 12$.

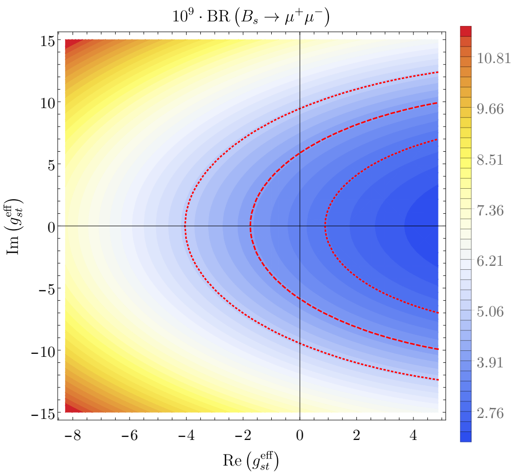

(e) $M_{H^\pm} = M_{H^0} = M_{A^0} = 2000\,\mathrm{GeV}$, $\tan\beta = 60$.

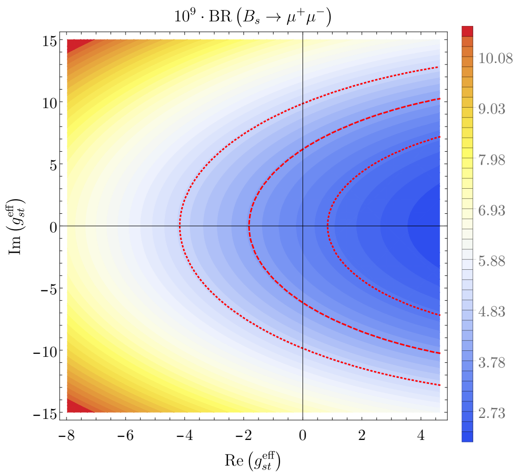

(f) $M_{H^\pm} = 1950\,\mathrm{GeV}$, $M_{H^0} = 2050\,\mathrm{GeV}$, $M_{A^0} = 2000\,\mathrm{GeV}$, $\tan\beta = 60$.

Figure 10. Same as Fig. 9 for the CMS branching ratio measurement [56].

parameter	numerical value	reference
M_{B_s}	$5.367\,\mathrm{GeV}$	[72]
m_b	$4.18\,\mathrm{GeV}$	[57]
m_s	$0.093\,\mathrm{GeV}$	[57]
m_μ	$0.106\,\mathrm{GeV}$	[73]
$\overline{m}_t\,(\overline{m}_t)$	$162.622\,\mathrm{GeV}$	[57]
$\alpha_s\,(M_Z = 91.1876\,\mathrm{GeV})$	0.1179	[57]
G_F	$1.166 \times 10^{-5}\,\mathrm{GeV}^{-2}$	[74]
M_W	$80.37\,\mathrm{GeV}$	[75]
f_{B_s}	$0.230\,\mathrm{GeV}$	[76]
Γ_H^s	$(1.616\,\mathrm{ps})^{-1}$	HFLAV
Γ_L^s	$(1.427\,\mathrm{ps})^{-1}$	HFLAV
$\lvert V_{ts}\rvert$	0.041	CKMfitter
$\lvert V_{tb}\rvert$	0.999	CKMfitter
$\lvert V_{cs}\rvert$	0.974	CKMfitter
$\lvert V_{cb}\rvert$	0.041	CKMfitter
$\mathcal{B}\,(B_s \to \mu^+\mu^-)_{\mathrm{SM}}$	$3.65(23) \times 10^{-9}$	[18]
$\mathcal{B}\,(B_s \to \mu^+\mu^-)_{\mathrm{LHCb}}$	$3.09^{+0.48}_{-0.44} \times 10^{-9}$	[54, 55]
$\mathcal{B}\,(B_s \to \mu^+\mu^-)_{\mathrm{CMS}}$	$3.95^{+0.52}_{-0.47} \times 10^{-9}$	[56]

Table 1. Numerical input used for the phenomenological analysis. For the QCD running of the top-quark mass and the renormalisation scale, we have used `RunDec` [77, 78]. The numerical values of the CKM matrix elements have been taken from the updates provided on the CKMfitter [79] web page. The numerical values of the B_s decay widths have been taken from the online updates provided at the HFLAV web page [58].

8 Summary

We have presented a 2HDM with three flavour-breaking spurions in the quark Yukawa sector. The model contains the established type-I and type-II models as limiting cases and otherwise permits large FCNC couplings in the up-type sector while naturally suppressing FCNC effects in down sector, as required by data. Despite the large number of parameters the model makes characteristic predictions, such as correlations between $b \to s\mu^+\mu^-$, $b \to s\gamma$, and $B_s - \bar{B}_s$ mixing, all of which involve the same combination g_{st}^{eff} of fundamental parameters. Also all couplings to right-handed down-type quarks are proportional to the quark masses as in the type-II model.

We have studied in detail the rare decay $B_s \to \mu^+\mu^-$, calculated the Wilson coefficients of the effective operators Q_S and Q_P, and demonstrated the consistency of the model by showing that the UV counterterms follow the pattern of the spurion expansion. Next we have calculated next-to-leading order (two-loop) QCD corrections to this process to (i) verify that higher-order QCD corrections can be correctly included (e.g. all UV divergences could be renormalised in the usual way plus countertems for our new couplings) and (ii) tame the sizable renormalisation-scale dependence of the Yukawa couplings. Then we have studied the phenomenology of an FCNC coupling g_{ct} of the heavy neutral Higgs bosons to top and charm quarks. We have found that —contrary to expectation— the dominant contribution to the loop-induced $\bar{s}_L b_R A^0$ and $\bar{s}_L b_R H^0$ couplings do not come from vertex diagrams with the neutral Higgs coupling to the internal top-charm line, but from charged-Higgs couplings which inherit the dependence on g_{ct} through SU(2) symmetry. The corresponding diagram (FCNC self-energy with the neutral Higgs attached to the b line) is enhanced by a factor of $\tan\beta$ compared to the vertex diagram, resulting in a $\mathcal{O}\left(\tan^3\beta\right)$ contribution to the $B_s \to \mu^+\mu^-$ amplitude which is absent in the type-II model. This feature makes $B_s \to \mu^+\mu^-$ a sensitive probe of the model even for Higgs masses well above the lower bounds found by the LHC experiments. For small Higgs masses, however, $b \to s\gamma$ precludes large effects in $B_s \to \mu^+\mu^-$. In our model the dominant contribution to $B_s - \bar{B}_s$ mixing is naturally small due to a suppression factor of $m_s m_b/v^2$; nevertheless $B_s - \bar{B}_s$ mixing sets constraints on the parameter space for very large Higgs masses.

Acknowledgments

M.L. would like to thank Florian Herren, Syuhei Iguro, Lucas Kunz and Mustafa Tabet for helpful discussions. The authors are grateful to Matthias Steinhauser for collaboration in an early stage of the project. This research was supported the BMBF grants 05H18VKCC1 and 05H21VKKBA as well as Deutsche Forschungsgemeinschaft (DFG, German Research Foundation) within the Collaborative Research Center *Particle Physics Phenomenology after the Higgs Discovery (P3H)* (project no. 396021762 – TRR 257). All Feynman diagrams within this paper have been produced using `TikZ-FeynHand` [80, 81].

References

[1] G.C. Branco, P.M. Ferreira, L. Lavoura, M.N. Rebelo, M. Sher and J.P. Silva, *Theory and phenomenology of two-Higgs-doublet models*, *Phys. Rept.* **516** (2012) 1 [1106.0034].

[2] J.F. Gunion, H.E. Haber, G.L. Kane and S. Dawson, *The Higgs Hunter's Guide*, vol. 80 (2000).

[3] J.E. Kim, *Light Pseudoscalars, Particle Physics and Cosmology*, *Phys. Rept.* **150** (1987) 1.

[4] R.D. Peccei and H.R. Quinn, *CP Conservation in the Presence of Instantons*, *Phys. Rev. Lett.* **38** (1977) 1440.

[5] R.D. Peccei and H.R. Quinn, *Constraints Imposed by CP Conservation in the Presence of Instantons*, *Phys. Rev. D* **16** (1977) 1791.

[6] H.E. Haber and G.L. Kane, *The Search for Supersymmetry: Probing Physics Beyond the Standard Model*, *Phys. Rept.* **117** (1985) 75.

[7] A. Crivellin, C. Greub and A. Kokulu, *Explaining $B \to D\tau\nu$, $B \to D^*\tau\nu$ and $B \to \tau\nu$ in a 2HDM of type III*, *Phys. Rev. D* **86** (2012) 054014 [1206.2634].

[8] A. Crivellin, A. Kokulu and C. Greub, *Flavor-phenomenology of two-Higgs-doublet models with generic Yukawa structure*, *Phys. Rev. D* **87** (2013) 094031 [1303.5877].

[9] T. Hermann, M. Misiak and M. Steinhauser, *Three-loop QCD corrections to $B_s \to \mu^+\mu^-$*, *JHEP* **12** (2013) 097 [1311.1347].

[10] C. Bobeth, M. Gorbahn and E. Stamou, *Electroweak Corrections to $B_{s,d} \to \ell^+\ell^-$*, *Phys. Rev. D* **89** (2014) 034023 [1311.1348].

[11] K. De Bruyn, R. Fleischer, R. Knegjens, P. Koppenburg, M. Merk and N. Tuning, *Branching Ratio Measurements of B_s Decays*, *Phys. Rev. D* **86** (2012) 014027 [1204.1735].

[12] K. De Bruyn, R. Fleischer, R. Knegjens, P. Koppenburg, M. Merk, A. Pellegrino et al., *Probing New Physics via the $B_s^0 \to \mu^+\mu^-$ Effective Lifetime*, *Phys. Rev. Lett.* **109** (2012) 041801 [1204.1737].

[13] H.E. Haber and D. O'Neil, *Basis-independent methods for the two-Higgs-doublet model. II. The Significance of tanβ*, *Phys. Rev. D* **74** (2006) 015018 [hep-ph/0602242].

[14] D. Eriksson, J. Rathsman and O. Stål, *2HDMC: Two-Higgs-Doublet Model Calculator Physics and Manual*, *Comput. Phys. Commun.* **181** (2010) 189 [0902.0851].

[15] G.C. Branco, L. Lavoura and J.P. Silva, *CP Violation*, vol. 103 (1999).

[16] M. Misiak and M. Steinhauser, *Weak radiative decays of the B meson and bounds on $M_{H^\pm}$ in the Two-Higgs-Doublet Model*, *Eur. Phys. J. C* **77** (2017) 201 [1702.04571].

[17] H.E. Logan and U. Nierste, *$B_{s,d} \to \ell^+\ell^-$ in a two Higgs doublet model*, *Nucl. Phys. B* **586** (2000) 39 [hep-ph/0004139].

[18] C. Bobeth, M. Gorbahn, T. Hermann, M. Misiak, E. Stamou and M. Steinhauser, *$B_{s,d} \to l^+l^-$ in the Standard Model with Reduced Theoretical Uncertainty*, *Phys. Rev. Lett.* **112** (2014) 101801 [1311.0903].

[19] T. Banks, *Supersymmetry and the Quark Mass Matrix*, *Nucl. Phys. B* **303** (1988) 172.

[20] L.J. Hall, R. Rattazzi and U. Sarid, *The Top quark mass in supersymmetric SO(10) unification*, *Phys. Rev. D* **50** (1994) 7048 [hep-ph/9306309].

[21] M. Carena, M. Olechowski, S. Pokorski and C.E.M. Wagner, *Electroweak symmetry breaking and bottom - top Yukawa unification*, *Nucl. Phys. B* **426** (1994) 269 [hep-ph/9402253].

[22] K.S. Babu and C.F. Kolda, *Higgs mediated $B^0 \to \mu^+\mu^-$ in minimal supersymmetry*, *Phys. Rev. Lett.* **84** (2000) 228 [hep-ph/9909476].

[23] G. Isidori and A. Retico, *Scalar flavor changing neutral currents in the large tan beta limit*, *JHEP* **11** (2001) 001 [hep-ph/0110121].

[24] A.J. Buras, P.H. Chankowski, J. Rosiek and Ł. Sławianowska, *$\Delta M_{d,s}, B^0 d, s \to \mu^+\mu^-$ and $B \to X_s\gamma$ in supersymmetry at large $\tan\beta$*, *Nucl. Phys. B* **659** (2003) 3 [hep-ph/0210145].

[25] A.J. Buras, P.H. Chankowski, J. Rosiek and Ł. Sławianowska, *Correlation between ΔM_s and $B^0_{s,d} \to \mu^+\mu^-$ in Supersymmetry at large $\tan\beta$*, *Phys. Lett.* **B546** (2002) 96 [hep-ph/0207241].

[26] L. Hofer, U. Nierste and D. Scherer, *Resummation of tan-beta-enhanced supersymmetric loop corrections beyond the decoupling limit*, *JHEP* **10** (2009) 081 [0907.5408].

[27] M. Gorbahn, S. Jäger, U. Nierste and S. Trine, *The supersymmetric Higgs sector and $B-\bar{B}$ mixing for large tan β*, *Phys. Rev. D* **84** (2011) 034030 [0901.2065].

[28] A. Dedes, H.K. Dreiner and U. Nierste, *Correlation of $B_s \to \mu^+\mu^-$ and (g-2) (μ) in minimal supergravity*, *Phys. Rev. Lett.* **87** (2001) 251804 [hep-ph/0108037].

[29] U. Nierste, M. Tabet and R. Ziegler, *Cornering Spontaneous CP Violation with Charged-Higgs-Boson Searches*, Phys. Rev. Lett. **125** (2020) 031801 [1912.11501].

[30] R.S. Chivukula and H. Georgi, *Composite Technicolor Standard Model*, Phys. Lett. B **188** (1987) 99.

[31] G. D'Ambrosio, G.F. Giudice, G. Isidori and A. Strumia, *Minimal flavor violation: An Effective field theory approach*, Nucl. Phys. B **645** (2002) 155 [hep-ph/0207036].

[32] P. Tuzon and A. Pich, *The Aligned two-Higgs Doublet model*, Acta Phys. Polon. Supp. **3** (2010) 215 [1001.0293].

[33] O. Eberhardt, A.P.n. Martínez and A. Pich, *Global fits in the Aligned Two-Higgs-Doublet model*, JHEP **05** (2021) 005 [2012.09200].

[34] N.D. Christensen, P. de Aquino, C. Degrande, C. Duhr, B. Fuks, M. Herquet et al., *A Comprehensive approach to new physics simulations*, Eur. Phys. J. C **71** (2011) 1541 [0906.2474].

[35] A. Alloul, N.D. Christensen, C. Degrande, C. Duhr and B. Fuks, *FeynRules 2.0 - A complete toolbox for tree-level phenomenology*, Comput. Phys. Commun. **185** (2014) 2250 [1310.1921].

[36] C. Degrande, C. Duhr, B. Fuks, D. Grellscheid, O. Mattelaer and T. Reiter, *UFO - The Universal FeynRules Output*, Comput. Phys. Commun. **183** (2012) 1201 [1108.2040].

[37] M. Gerlach, F. Herren and M. Lang, *tapir: A tool for topologies, amplitudes, partial fraction decomposition and input for reductions*, Comput. Phys. Commun. **282** (2023) 108544 [2201.05618].

[38] P. Nogueira, *Automatic Feynman graph generation*, J. Comput. Phys. **105** (1993) 279.

[39] B. Ruijl, T. Ueda and J. Vermaseren, *FORM version 4.2*, 1707.06453.

[40] R. Harlander, T. Seidensticker and M. Steinhauser, *Complete corrections of Order alpha alpha-s to the decay of the Z boson into bottom quarks*, Phys. Lett. B **426** (1998) 125 [hep-ph/9712228].

[41] T. Seidensticker, *Automatic application of successive asymptotic expansions of Feynman diagrams*, in *6th International Workshop on New Computing Techniques in Physics Research: Software Engineering, Artificial Intelligence Neural Nets, Genetic Algorithms, Symbolic Algebra, Automatic Calculation*, 5, 1999 [hep-ph/9905298].

[42] A.I. Davydychev and J.B. Tausk, *Two loop selfenergy diagrams with different masses and the momentum expansion*, Nucl. Phys. B **397** (1993) 123.

[43] J.E. Salomon, *Das Laufen und die Vereinigung der Eichkopplungen des Standardmodells zur Drei-Schleifen-Ordnung*, Ph.D. thesis, KIT, Karlsruhe, 2012. 10.5445/IR/1000030116.

[44] T. Inami and C.S. Lim, *Effects of Superheavy Quarks and Leptons in Low-Energy Weak Processes $K_L \to \mu\bar{\mu}$, $K^+ \to \pi + \nu\bar{\nu}$ and $K^0 \leftrightarrow \bar{K}^0$*, Progress of Theoretical Physics **65** (1981) 297 [https://academic.oup.com/ptp/article-pdf/65/1/297/5252099/65-1-297.pdf].

[45] G. Buchalla and A.J. Buras, *QCD corrections to the sdZ vertex for arbitrary top quark mass*, Nuclear Physics B **398** (1993) 285.

[46] G. Buchalla and A.J. Buras, *QCD corrections to rare K- and B-decays for arbitrary top quark mass*, Nuclear Physics B **400** (1993) 225.

[47] G. Buchalla and A.J. Buras, *The rare decays $K \to \pi\nu\bar{\nu}$, $B \to X\nu\bar{\nu}$ and $B \to l^+l^-$: An Update*, Nucl. Phys. B **548** (1999) 309 [hep-ph/9901288].

[48] M. Misiak and J. Urban, *QCD corrections to FCNC decays mediated by Z penguins and W boxes*, Phys. Lett. B **451** (1999) 161 [hep-ph/9901278].

[49] M. Beneke, C. Bobeth and R. Szafron, *Enhanced electromagnetic correction to the rare B-meson decay* $B_{s,d} \to \mu^+\mu^-$, Phys. Rev. Lett. **120** (2018) 011801 [1708.09152].

[50] M. Beneke, C. Bobeth and R. Szafron, *Power-enhanced leading-logarithmic QED corrections to* $B_q \to \mu^+\mu^-$, JHEP **10** (2019) 232 [1908.07011].

[51] C. Bobeth, T. Ewerth, F. Krüger and J. Urban, *Analysis of neutral Higgs boson contributions to the decays* $\bar{B}(\,s) \to \ell^+\ell^-$ *and* $\bar{B} \to K\ell^+\ell^-$, Phys. Rev. D **64** (2001) 074014 [hep-ph/0104284].

[52] C. Bobeth, A.J. Buras, F. Krüger and J. Urban, *QCD corrections to* $\bar{B} \to X_{d,s}\nu\bar{\nu}$, $\bar{B}_{d,s} \to \ell^+\ell^-$, $K \to \pi\nu\bar{\nu}$ *and* $K_L \to \mu^+\mu^-$ *in the MSSM*, Nucl. Phys. B **630** (2002) 87 [hep-ph/0112305].

[53] T. Hermann, *Seltene B-Meson-Zerfälle innerhalb und jenseits des Standardmodells*, Ph.D. thesis, KIT, Karlsruhe, 2014. 10.5445/IR/1000041138.

[54] LHCb collaboration, *Analysis of Neutral B-Meson Decays into Two Muons*, Phys. Rev. Lett. **128** (2022) 041801 [2108.09284].

[55] LHCb collaboration, *Measurement of the* $B_s^0 \to \mu^+\mu^-$ *decay properties and search for the* $B^0 \to \mu^+\mu^-$ *and* $B_s^0 \to \mu^+\mu^-\gamma$ *decays*, Phys. Rev. D **105** (2022) 012010 [2108.09283].

[56] CMS collaboration, *Measurement of* $\mathrm{B_s^0} \to \mu^+\mu^-$ *decay properties and search for the* $\mathrm{B^0} \to \mu\mu$ *decay in proton-proton collisions at* $\sqrt{s} = 13$ TeV, *report CMS-PAS-BPH-21-006*, .

[57] Particle Data Group collaboration, *Review of Particle Physics*, PTEP **2020** (2020) 083C01.

[58] HFLAV collaboration, *Averages of b-hadron, c-hadron, and* τ*-lepton properties as of 2018*, Eur. Phys. J. C **81** (2021) 226 [1909.12524].

[59] M. Blanke and S. Iguro, *Collider probe of heavy additional Higgs bosons solving the muon* $g-2$, 2210.13508.

[60] M. Blanke, A. Crivellin, S. de Boer, T. Kitahara, M. Moscati, U. Nierste et al., *Impact of polarization observables and* $B_c \to \tau\nu$ *on new physics explanations of the* $b \to c\tau\nu$ *anomaly*, Phys. Rev. D **99** (2019) 075006 [1811.09603].

[61] M. Blanke, A. Crivellin, T. Kitahara, M. Moscati, U. Nierste and I. Nišandžić, *Addendum to "Impact of polarization observables and* $B_c \to \tau\nu$ *on new physics explanations of the* $b \to c\tau\nu$ *anomaly"*, 1905.08253.

[62] LHCb collaboration, "First joint measurement of $r(d^*)$ and $r(d^0)$ at lhcb." https://indico.cern.ch/event/1187939/.

[63] S. Iguro, T. Kitahara and R. Watanabe, *Global fit to* $b \to c\tau\nu$ *anomalies 2022 mid-autumn*, 2210.10751.

[64] M. Fedele, M. Blanke, A. Crivellin, S. Iguro, T. Kitahara, U. Nierste et al., *Impact of* $\Lambda_b \to \Lambda_c\tau\nu$ *measurement on New Physics in* $b \to c\,l\nu$ *transitions*, 2211.14172.

[65] ATLAS collaboration, *Search for charged Higgs bosons decaying via* $H^\pm \to \tau^\pm\nu_\tau$ *in the* τ*+jets and* τ*+lepton final states with 36 fb*$^{-1}$ *of pp collision data recorded at* $\sqrt{s} = 13$ *TeV with the ATLAS experiment*, JHEP **09** (2018) 139 [1807.07915].

[66] ATLAS collaboration, *Summary plots for beyond Standard Model Higgs boson benchmarks for direct and indirect searches, ATLAS UB note ATL-PHYS-PUB-2022-043.*, .

[67] ATLAS collaboration, *Combined measurements of Higgs boson production and decay using up to 80 fb^{-1} of proton-proton collision data at $\sqrt{s} = 13$ TeV collected with the ATLAS experiment*, Phys. Rev. D **101** (2020) 012002 [1909.02845].

[68] CMS collaboration, *Combined measurements of Higgs boson couplings in proton–proton collisions at $\sqrt{s} = 13$ TeV*, Eur. Phys. J. C **79** (2019) 421 [1809.10733].

[69] T. Hermann, M. Misiak and M. Steinhauser, *$\bar{B} \to X_s\gamma$ in the Two Higgs Doublet Model up to Next-to-Next-to-Leading Order in QCD*, JHEP **11** (2012) 036 [1208.2788].

[70] M. Misiak et al., *Updated NNLO QCD predictions for the weak radiative B-meson decays*, Phys. Rev. Lett. **114** (2015) 221801 [1503.01789].

[71] V. Cacchio, D. Chowdhury, O. Eberhardt and C.W. Murphy, *Next-to-leading order unitarity fits in Two-Higgs-Doublet models with soft $\mathbb{Z}_2$ breaking*, JHEP **11** (2016) 026 [1609.01290].

[72] LHCb collaboration, *Observation of $B^0_{(s)} \to J/\psi p\bar{p}$ decays and precision measurements of the $B^0_{(s)}$ masses*, Phys. Rev. Lett. **122** (2019) 191804 [1902.05588].

[73] P.J. Mohr, D.B. Newell and B.N. Taylor, *CODATA Recommended Values of the Fundamental Physical Constants: 2014*, Rev. Mod. Phys. **88** (2016) 035009 [1507.07956].

[74] MuLan collaboration, *Measurement of the Positive Muon Lifetime and Determination of the Fermi Constant to Part-per-Million Precision*, Phys. Rev. Lett. **106** (2011) 041803 [1010.0991].

[75] ATLAS collaboration, *Measurement of the W-boson mass in pp collisions at $\sqrt{s} = 7$ TeV with the ATLAS detector*, Eur. Phys. J. C **78** (2018) 110 [1701.07240].

[76] Y. Aoki et al., *FLAG Review 2021*, 2111.09849.

[77] K.G. Chetyrkin, J.H. Kühn and M. Steinhauser, *RunDec: A Mathematica package for running and decoupling of the strong coupling and quark masses*, Comput. Phys. Commun. **133** (2000) 43 [hep-ph/0004189].

[78] F. Herren and M. Steinhauser, *Version 3 of RunDec and CRunDec*, Comput. Phys. Commun. **224** (2018) 333 [1703.03751].

[79] CKMfitter Group collaboration, *CP violation and the CKM matrix: Assessing the impact of the asymmetric B factories*, Eur. Phys. J. C **41** (2005) 1 [hep-ph/0406184].

[80] M. Dohse, *TikZ-FeynHand: Basic User Guide*, 1802.00689.

[81] J. Ellis, *TikZ-Feynman: Feynman diagrams with TikZ*, Comput. Phys. Commun. **210** (2017) 103 [1601.05437].